INSTITUTE OF PHYSICS
FACULTY OF PHYSICS, ASTRONOMY
AND APPLIED COMPUTER SCIENCE
JAGIELLONIAN UNIVERSITY

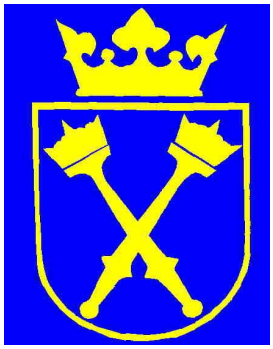

Diploma Thesis

Investigations of the time interval distributions between the decays of quantum entangled neutral kaons

Tomasz Twaróg

Supervisor: Professor Paweł Moskal

Cracow, 2010

Acknowledgements

First of all, I would like to express my deepest gratitude towards Professor Paweł Moskal for constant encouragement, endless patience and suggestions about the form and contents of this thesis.

I thank Professor Wojciech Wiślicki for our regular Skype conversations, many helpful suggestions and explanations.

I am also indebted to Professor Antonio Di Domenico for his hospitality during my stays at Laboratori Nazionali di Frascati, for organising financial support from Sapienza University of Rome and for finding time to answer my questions despite his busy schedule.

I would like to thank Professor Bogusław Kamys for financial support of my stays in Frascati.

The work is easier with a good company. I thank Dagmara Rozpędzik, Izabela Balwierz, Magdalena Skurzok, Michał Silarski, Gzegorz Wyszyński, Tomasz Bednarski and Szymon Niedźwiecki for a nice atmosphere during the daily work at the university.

During writing this thesis I spent quite a lot of time in Frascati. For the similar reason as above I should thank Erika De Lucia, Antonio De Santis, Marek Jacewicz and many others.

Eryk Czerwiński and Jarosław Zdebik were always eager to help me both in Kraków and in Frascati. Thanks a lot.

I would like to cordially thank my whole family for the support I have been receiving for my entire life.

Last but not least, I thank Ewa Tertil for her care and support during the last years.

Abstract

Investigations of the time interval distributions between the decays of quantum entangled neutral kaons

Since their discovery, kaons have unabatedly attracted interest of particle physics researchers. As the lightest flavoured particles, they offer an excellent possibility of testing discrete symmetries. KLOE experiment at DAΦNE facility in Frascati (Italy) stands out among others. It allows to reach incomparable precision in CPT symmetry and quantum mechanics tests.

KLOE owes its uniqueness to the fact that DAΦNE produces neutral kaons in quantum entangled pairs. In this work a detailed derivation of formulae for double decay rate from the initial two kaons state is presented. The results are then applied to specific final states. Emphasis is given to connection between the decay intensities and symmetries.

Although there has been no evidence of CPT symmetry breaking, several parameterisations have been proposed where this symmetry is not fundamental and thus can be violated. One of these ideas is the CPT noninvariance due to evolution of pure into mixed states induced by quantum gravity effects, which at the same time happens to be inconsistent with quantum mechanics. This concept is shortly presented.

A subset of KLOE data is analysed for the symptoms of decoherence caused by the aforementioned mechanism. For reasons referred to in the text the results obtained in this work are less significant than those from KLOE analysis, nonetheless their orders of magnitude indicate the expediency of further measurements.

Contents

1 Introduction

Kaons (also called K mesons) are the lightest particles containing a strange quark, s, apart from the most common quarks u (up) or d (down), and for this reason their potential for testing fundamental physics laws was realised almost from the moment of their discovery. The behaviour of charged kaons served as an inspiration for Lee and Yang to propose experiments testing parity conservation [1]. Neutral kaons were particles for which CP [2] and T [3] violations were first observed. Then it should not come as a surprise that they are promising candidates in the search of CPT noninvariance.

CPT symmetry is a combination of three discrete symmetries: $P-$ parity, $C-$ charge conjugation and $T-$ time reversal, and although P, C and T have all been shown to be violated individually, CPT symmetry seems to remain intact. It was shown by Pauli [4] to hold for any quantum field theory and for any order of the C, P and T transformations under very basic assumptions: Lorentz invariance, unitarity (conservation of probability) and locality. There was an earlier, but less general proof by Lüders [5].

This work deals with a system of two neutral kaons produced in a ϕ meson decay. Such pairs are produced at DAΦNE, Frascati ϕ-factory. A system of two neutral kaons has been called one of the most intriguing in nature for quite a long time [6, 7] and it is definitely worth investigating into, and not only because it allows testing symmetries. The necessity to conserve parity and charge conjugation eigenvalues in ϕ decays leads to expressions which straightforwardly suggest quantum mechanics tests through the phenomenon called quantum entanglement.

The goal of this thesis is to show how, starting from very basic assumptions, one can deduce about neutral kaons system properties basing on the time intervals between the decays of quantum entangled kaons. This is done on a more basic level than usually presented in papers, hence it allows even a reader who is less familiar with the subject to follow the arguments. In case of doubts, many calculations are included in the appendix.

The other topic considered, which also is of great interest, is the analysis of possible CPT symmetry and quantum mechanics violation in the neutral kaons system. Among sources proposed to possibly lead to this yet unobserved violations is the evolution of pure states into mixed states. A suitable parameterisation of double decay rates and results of analysis of KLOE data from the year 2005 are presented. However, results obtained in this work should not be compared directly to KLOE ones, as there were differences in the fitting methods used. These differences will be emphasized in the text.

2 Neutral kaons system

2.1 Hamiltonian

At the moment of production, neutral kaon is a superposition of K^0 and $\bar{K}^0$ states:

$$|K(0)\rangle = a(0)\left|K^0\right\rangle + b(0)\left|\bar{K}^0\right\rangle, \tag{1}$$

while its time evolution can be described as:

$$|K(t)\rangle = a(t)\left|K^0\right\rangle + b(t)\left|\bar{K}^0\right\rangle + \sum_j c_j(t)\left|f_j\right\rangle, \tag{2}$$

where the sum is over all final states $|f_j\rangle$ a kaon may decay to. As the functions a and b are time-dependent, it follows from this formula that a neutral kaon can oscillate between $\left|K^0\right\rangle$ and $\left|\bar{K}^0\right\rangle$ states, which in fact happens with a frequency of about 5.3 GHz, being a second-order weak process with strangeness change $|\Delta S| = 2$. Phenomenology of the neutral kaons system is successfully described by the Wigner-Weisskopf approximation [8]. Although studies of possible deviations from this approximation have been performed, further tests are desirable as the effects that are searched for in K^0-$\bar{K}^0$ complex are very tiny [9]. With the help of Wigner-Weisskopf approximation one finds that the functions $a(t)$ and $b(t)$ obey the Schrödinger-like equation with effective Hamiltonian $\mathbf{H}$ [7]:

$$i\frac{\partial}{\partial t}\begin{pmatrix} a(t) \\ b(t) \end{pmatrix} = \mathbf{H}\begin{pmatrix} a(t) \\ b(t) \end{pmatrix}. \tag{3}$$

Let us denote $\psi = e^{-i\mathbf{H}t}\psi_0$ with $\psi_0 = \psi(t=0)$. Since the kaons decay, we have the condition $0 > \frac{d|\psi|^2}{dt}$, and by writing the wave function more explicitly we obtain:

$$\begin{aligned} 0 > \frac{d\left(\psi^\dagger\psi\right)}{dt} =& \psi^\dagger\frac{d\psi}{dt} + \frac{d\psi^\dagger}{dt}\psi = \psi^\dagger\left(-i\mathbf{H}\right)e^{-i\mathbf{H}t}\psi_0 + \psi_0^\dagger i\mathbf{H}^\dagger e^{i\mathbf{H}^\dagger t}\psi = \\ =& -i\psi^\dagger\left(\mathbf{H} - \mathbf{H}^\dagger\right)\psi, \end{aligned} \tag{4}$$

so clearly $\mathbf{H}$ is not hermitian. However, in general any complex matrix can be divided into its hermitian and antihermitian parts. In this particular case we write:

$$\mathbf{H} = \mathbf{M} - \frac{i}{2}\mathbf{\Gamma} = \begin{pmatrix} M_{11} & M_{12} \\ M_{12}^* & M_{22} \end{pmatrix} - \frac{i}{2}\begin{pmatrix} \Gamma_{11} & \Gamma_{12} \\ \Gamma_{12}^* & \Gamma_{22} \end{pmatrix}, \tag{5}$$

where $\mathbf{M}$ and $\mathbf{\Gamma}$ are hermitian and are called mass and decay matrices, respectively. Elements M_{11} and Γ_{11} can be associated with K^0, while M_{22} and Γ_{22} can be linked with $\bar{K}^0$. It should be expected that the decay part leads to exponential damping, hence the minus sign and the factor $\frac{1}{2}$ (the dependence on time will be of the usual form $\psi \sim e^{-iEt} = e^{-i(m-i\Gamma/2)t} = e^{-imt}e^{-\Gamma t/2}$, so $|\psi|^2 \sim e^{-\Gamma t}$).

2.2 Symmetries

In this section connection between symmetries in the neutral kaons system and Hamiltonian matrix elements is discussed.

2.2.1 CPT

One of the consequences of the CPT theorem is that masses and widths of particles and their antiparticles are the same, so in this case $m_{K^0} = m_{\bar{K}^0}$ and $\Gamma_{K^0} = \Gamma_{\bar{K}^0}$. In addition to this, CPT symmetry ensures that probabilities of transitions $K^0 \to K^0$ and $\bar{K}^0 \to \bar{K}^0$ at a given time are the same. For Hamiltonian matrix (5) this implies:

$$CPT: \qquad M_{11} = M_{22}, \qquad \Gamma_{11} = \Gamma_{22}; \qquad H_{11} = H_{22}. \tag{6}$$

2.2.2 T

Symmetry with respect to time reversal implies that transitions $K^0 \to \bar{K}^0$ and $\bar{K}^0 \to K^0$ at a given time have the same probabilities. In the Hamiltonian matrix (5) elements responsible for these transitions are H_{12} and H_{21}. Therefore we have:

$$T: \qquad |H_{12}| = |H_{21}|\,. \tag{7}$$

2.2.3 CP

An additional hierarchy among the symmetry violations is introduced by quantum mechanics for a two-state systems: the detection of a violation of the CPT or (and) of the T symmetry implies a CP symmetry violation [10]. Hence we have:

$$CP: \qquad H_{11} = H_{22} \qquad \text{and} \qquad |H_{12}| = |H_{21}|\,. \tag{8}$$

2.3 Eigenvalues, eigenstates

The equation for eigenvalues of the Hamiltonian is generic (for slightly richer calculations used for this section refer to A.1.1):

$$\det\left(\mathbf{H} - \lambda\mathbf{1}\right) = 0, \tag{9}$$

from which it is straightforward to obtain:

$$\lambda^2 - \lambda\left(H_{11} + H_{22}\right) + H_{11}H_{22} - H_{12}H_{21} = 0. \tag{10}$$

From the equation above one finds the discriminant:

$$\Delta = \left(H_{11} - H_{22}\right)^2 + 4H_{12}H_{21}. \tag{11}$$

From this we find the eigenvalues of $\mathbf{H}$ in the limit of CP and CPT (refer to section A.1.1 for more details):

$$\lambda_\pm = \frac{1}{2}\left(H_{11} + H_{22} \pm \sqrt{4H_{12}H_{21}}\right) \overset{CPT}{=\!=} H_{11} \pm \sqrt{H_{12}H_{21}}, \tag{12}$$

where the square root, written explicitly in terms of M_{12} and Γ_{12}, is:

$$\sqrt{H_{12}H_{21}} = \sqrt{|M_{12}|^2 + \frac{1}{4}|\Gamma_{12}|^2}\exp\left[-\frac{i}{2}\arcsin\left(\frac{|M_{12}\Gamma_{12}|}{|M_{12}|^2 + \frac{1}{4}|\Gamma_{12}|^2}\right)\right]. \tag{13}$$

Having the eigenvalues we proceed to calculate the eigenstates of $\mathbf{H}$ (slightly richer calculations are included in section A.1.2). Equation for eigenstates is generic:

$$\begin{pmatrix} H_{11} - \lambda_\pm & H_{12} \\ H_{21} & H_{22} - \lambda_\pm \end{pmatrix} v_\pm = 0. \tag{14}$$

If one defines:

$$v_\pm \overset{def}{=\!=} \begin{pmatrix} u_\pm \\ w_\pm \end{pmatrix} \qquad \text{and} \qquad e^{-2i\alpha} \overset{def}{=\!=} \frac{H_{12}}{H_{21}},$$

the eigenvectors can be shown to be of the form:

$$\begin{aligned} v_+ &= u_+ e^{i\frac{\alpha}{2}} \begin{pmatrix} e^{-i\frac{\alpha}{2}} \\ e^{i\frac{\alpha}{2}} \end{pmatrix}, \\ v_- &= -w_- e^{-i\frac{\alpha}{2}} \begin{pmatrix} e^{-i\frac{\alpha}{2}} \\ -e^{i\frac{\alpha}{2}} \end{pmatrix}. \end{aligned} \tag{15}$$

One can note that v_+ and v_- are $CP-$even and $CP-$odd, respectively [11]. Therefore by continuity we identify:

$$v_+ \equiv |K_S\rangle, \qquad v_- \equiv |K_L\rangle\,; \tag{16}$$

$$\lambda_+ \equiv \lambda_S = m_S - i\frac{\Gamma_S}{2}, \qquad \lambda_- \equiv \lambda_L = m_L - i\frac{\Gamma_L}{2}. \tag{17}$$

The short- and long-lived $|K_S\rangle$ and $|K_L\rangle$ states are commonly expressed as:

$$\begin{aligned} |K_S\rangle =& \frac{1}{\sqrt{2\left(1+|\epsilon_S|^2\right)}}\left[(1+\epsilon_S)\left|K^0\right\rangle + (1-\epsilon_S)\left|\bar{K}^0\right\rangle\right], \\ |K_L\rangle =& \frac{1}{\sqrt{2\left(1+|\epsilon_L|^2\right)}}\left[(1+\epsilon_L)\left|K^0\right\rangle - (1-\epsilon_L)\left|\bar{K}^0\right\rangle\right]. \end{aligned} \tag{18}$$

Additional information about the mass difference between these particles, their mean lifetimes and main decay modes is provided in Tab. 1. In the equations above ϵ_S and ϵ_L are small (of the order 10^{-3}), complex parameters measuring CP violation for K_S and K_L. Another pair of parameters can be equivalently defined:

$$\bar{\epsilon} \equiv \frac{\epsilon_S + \epsilon_L}{2}, \tag{19}$$

$$\delta \equiv \frac{\epsilon_S - \epsilon_L}{2}. \tag{20}$$

$\bar{\epsilon}$ informs about average CP violation for neutral kaons, while δ is a CPT-violating parameter which will be useful later.

Table 1: Selected information about K_S and K_L particles. The data are extracted from [12].

Parameter	K_S	K_L
lifetime	(89.58 ± 0.05) ps	(51.16 ± 0.20) ns
mass difference, $m_L - m_S$	$(3.4819 \pm 0.0099)\cdot 10^{-6}$ eV	
main decay modes, Γ_i/Γ	$\pi^+\pi^-$ 0.6920 ± 0.0005	$\pi^\pm e^\mp \nu_e$ 0.4055 ± 0.0012
	$\pi^0\pi^0$ 0.3069 ± 0.0005	$\pi^\pm \mu^\mp \nu_\mu$ 0.2704 ± 0.0007
	$\pi^+\pi^-\gamma$ $(1.79 \pm 0.05)\cdot 10^{-3}$	$3\pi^0$ 0.1952 ± 0.0012
	$\pi^\pm e^\mp \nu_e$ $(7.04 \pm 0.08)\cdot 10^{-4}$	$\pi^+\pi^-\pi^0$ 0.1254 ± 0.0005
	$\pi^\pm \mu^\mp \nu_\mu$ $(4.69 \pm 0.05)\cdot 10^{-4}$	$\pi^+\pi^-$ $(1.966 \pm 0.010)\cdot 10^{-3}$
		$\pi^0\pi^0$ $(8.65 \pm 0.06)\cdot 10^{-4}$

3 Final states amplitudes for $\phi \to K^0\bar{K}^0 \to f_1 f_2$

At KLOE, neutral kaons are produced in ϕ meson decay, $J^{PC} = 1^{--}$, with a 33.8% probability (for the list of the main ϕ decay modes, see Tab. 2).

Table 2: Main ϕ decay modes.

Decay mode	Branching ratio (%) [12]
K^+K^-	49.1
$K^0\bar{K}^0$	33.8
$\rho\pi + \pi^+\pi^-\pi^0$	15.6
$\eta\gamma$	1.26

To conserve the eigenvalues of P and C, the (normalized) initial state of the two kaons, written in the ϕ rest frame, has to be:

$$|i\rangle = \frac{1}{\sqrt{2}}\{\left|K^0\left(-\vec{p}\right)\right\rangle \left|\bar{K}^0\left(+\vec{p}\right)\right\rangle - \left|\bar{K}^0\left(-\vec{p}\right)\right\rangle \left|K^0\left(+\vec{p}\right)\right\rangle\}. \tag{21}$$

It is easy to show that $C\,|i\rangle = -\,|i\rangle$ and $P\,|i\rangle = -\,|i\rangle$, as required.

We can change the basis of strangeness eigenstates (suitable for the description of kaon pair production), $\{\left|K^0\right\rangle, \left|\bar{K}^0\right\rangle\}$, to the basis of Hamiltonian eigenstates suitable for the description of the decays, $\{|K_S\rangle, |K_L\rangle\}$ (refer to A.2.1 for precise calculations):

$$|i\rangle = \frac{N}{\sqrt{2}}\{|K_S\left(+\vec{p}\right)\rangle |K_L\left(-\vec{p}\right)\rangle - |K_L\left(+\vec{p}\right)\rangle |K_S\left(-\vec{p}\right)\rangle\}, \tag{22}$$

where

$$N = \frac{\sqrt{\left(1+|\epsilon_S|^2\right)\left(1+|\epsilon_L|^2\right)}}{1-\epsilon_S\epsilon_L} \approx 1 \tag{23}$$

is a normalization factor.

Given eq. (22), one can calculate a general formula for the double decay rate of the initial two kaons state, which will be done in the following section. Later a specific case of two identical final states is discussed (section 3.2), and finally two (out of many) interesting examples of different final states are presented in section 3.3.

3.1 General case

Following quantum mechanics rules, the decay amplitude of the two kaons state (22) into final states f_1 and f_2 at times t_1 and t_2 and momenta $+\vec{p}$ and $-\vec{p}$, respectively, can be expressed as:

$$\begin{aligned}
A\left(f_1,t_1;f_2,t_2\right) &= \frac{N}{\sqrt{2}}\{\langle f_1|T|K_S\left(t_1\right)\rangle \langle f_2|T|K_L\left(t_2\right)\rangle + \\
&\quad - \langle f_1|T|K_L\left(t_1\right)\rangle \langle f_2|T|K_S\left(t_2\right)\rangle\} = \\
&= \frac{N}{\sqrt{2}}\{\langle f_1|T|K_S\rangle \langle f_2|T|K_L\rangle e^{-i\lambda_S t_1} e^{-i\lambda_L t_2} + \\
&\quad - \langle f_1|T|K_L\rangle \langle f_2|T|K_S\rangle e^{-i\lambda_L t_1} e^{-i\lambda_S t_2}\} = \\
&= \frac{N}{\sqrt{2}}\{\langle f_1|T|K_S\rangle \langle f_2|T|K_L\rangle e^{-im_S t_1} e^{-\frac{1}{2}\Gamma_S t_1} e^{-im_L t_2} e^{-\frac{1}{2}\Gamma_L t_2} + \\
&\quad - \langle f_1|T|K_L\rangle \langle f_2|T|K_S\rangle e^{-im_L t_1} e^{-\frac{1}{2}\Gamma_L t_1} e^{-im_S t_2} e^{-\frac{1}{2}\Gamma_S t_2}\},
\end{aligned} \tag{24}$$

where T is an operator whose explicit form is unknown, but also not needed here.

The complex conjunction of this amplitude reads:

$$\begin{aligned} A^*(f_1,t_1;f_2,t_2) =& \frac{N^*}{\sqrt{2}}\{\langle f_1|T|K_S\rangle^* \langle f_2|T|K_L\rangle^* e^{im_S t_1} e^{-\frac{1}{2}\Gamma_S t_1} e^{im_L t_2} e^{-\frac{1}{2}\Gamma_L t_2} + \\ & - \langle f_1|T|K_L\rangle^* \langle f_2|T|K_S\rangle^* e^{im_L t_1} e^{-\frac{1}{2}\Gamma_L t_1} e^{im_S t_2} e^{-\frac{1}{2}\Gamma_S t_2}\}. \end{aligned} \tag{25}$$

The double decay rate of the two kaons into f_1 and f_2 correspondingly at times t_1 and t_2 can now be calculated (detailed calculations can be found in A.2.2):

$$\begin{aligned} I(f_1,t_1;f_2,t_2) &= |A(f_1,t_1;f_2,t_2)|^2 = A(f_1,t_1;f_2,t_2)\, A^*(f_1,t_1;f_2,t_2) = \\ &= C_{12}\{|\eta_1|^2 e^{-\Gamma_L t_1 - \Gamma_S t_2} + |\eta_2|^2 e^{-\Gamma_S t_1 - \Gamma_L t_2} + \\ &\quad - 2|\eta_1||\eta_2| e^{-\frac{\Gamma_S+\Gamma_L}{2}(t_1-t_2)} \cos[\Delta m (t_1-t_2) + \phi_2 - \phi_1]\}, \end{aligned} \tag{26}$$

where we have denoted:

$$C_{12} = \frac{|N|^2}{2} |\langle f_1|T|K_S\rangle \langle f_2|T|K_S\rangle|^2 \tag{27}$$

and introduced decay amplitude ratios η_i:

$$\eta_i = |\eta_i| e^{i\phi_i} \equiv \frac{\langle f_i|T|K_L\rangle}{\langle f_i|T|K_S\rangle}. \tag{28}$$

Experimental data may be easier to compare with one-dimensional time distributions, when difference $\Delta t = t_1 - t_2$ is used instead of decay times t_1 and t_2. To find the Δt distribution it is necessary to change variables to $t = t_1 + t_2$ (the simplest choice) and Δt and then integrate the obtained formula over t (see A.2.3 for additional comments and calculations). The results for positive and negative Δt are as follows:

$$\begin{aligned} I(f_1,f_2,\Delta t \geq 0) = \frac{C_{12}}{\Gamma_S+\Gamma_L}\{&|\eta_1|^2 e^{-\Gamma_L \Delta t} + |\eta_2|^2 e^{-\Gamma_S \Delta t} + \\ &- 2|\eta_1||\eta_2| e^{-\frac{\Gamma_S+\Gamma_L}{2}\Delta t} \cos[\Delta m \Delta t + \phi_2 - \phi_1]\}, \end{aligned} \tag{29}$$

$$\begin{aligned} I(f_1,f_2,\Delta t \leq 0) = \frac{C_{12}}{\Gamma_S+\Gamma_L}\{&|\eta_1|^2 e^{-\Gamma_S |\Delta t|} + |\eta_2|^2 e^{-\Gamma_L |\Delta t|} + \\ &- 2|\eta_1||\eta_2| e^{-\frac{\Gamma_L+\Gamma_S}{2}|\Delta t|} \cos[\Delta m |\Delta t| + \phi_1 - \phi_2]\}. \end{aligned} \tag{30}$$

3.2 Identical final states

In the case when final states f_1 and f_2 are the same, eqs. (29) and (30) are significantly simplified. Straight from eq. (28) we have $\eta_1 = \eta_2$, so in particular $|\eta_1| = |\eta_2|$ and $\phi_1 = \phi_2$. Eqs. (29) and (30) become:

$$\begin{aligned} I(f_1 = f_2, \Delta t \geq 0) &= I(f_1 = f_2, \Delta t \leq 0) = \\ &= \frac{C_{12}|\eta|^2}{\Gamma_S+\Gamma_L}\{e^{-\Gamma_L|\Delta t|} + e^{-\Gamma_S|\Delta t|} - 2e^{-\frac{\Gamma_S+\Gamma_L}{2}|\Delta t|} \cos(\Delta m |\Delta t|)\}\ , \end{aligned} \tag{31}$$

where eta's subscript is omitted for simplicity. It is clear that function I is even in Δt. It is also visible that the shape of the curve I does not depend on the choice of final states as long as they are the same. There are two regions of particular interest. The first one, around $4\tau_S$, is the most sensitive to Δm value, as presented in Fig. 1 on page 14. The second one is close to $\Delta t = 0$. We easily see that:

$$I(f_1 = f_2, \Delta t = 0) = \frac{C_{12}|\eta|^2}{\Gamma_S+\Gamma_L}\{1 + 1 - 2\} = 0.$$

Therefore, for identical final states, no events are expected in $\Delta t = 0$ within the scope of quantum mechanics. Decays to identical final states are described further in chapter 4.

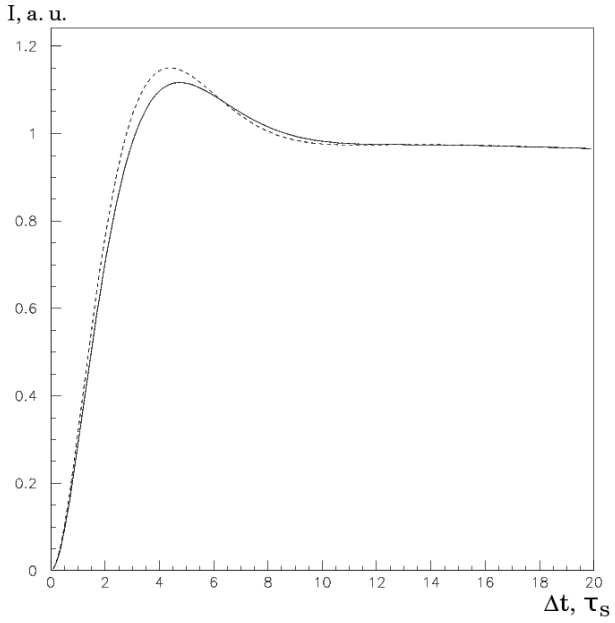

Figure 1: Double decay rate as a function of Δt for identical final states. The solid curve is for current Δm value, while the dashed line is for Δm 10% bigger. It can be seen that the most sensitive region for Δm is around the interference peak ($\sim 4\tau_S$).

3.3 Other useful final states

3.3.1 Double semileptonic final state

We proceed to discuss a situation, in which both kaons decay via semileptonic channel, but to different final states. This means that the products of the decay are $\pi^+ l^- \bar{\nu}$ and $\pi^- l^+ \nu$, where l can be either an electron (positron) or a muon.

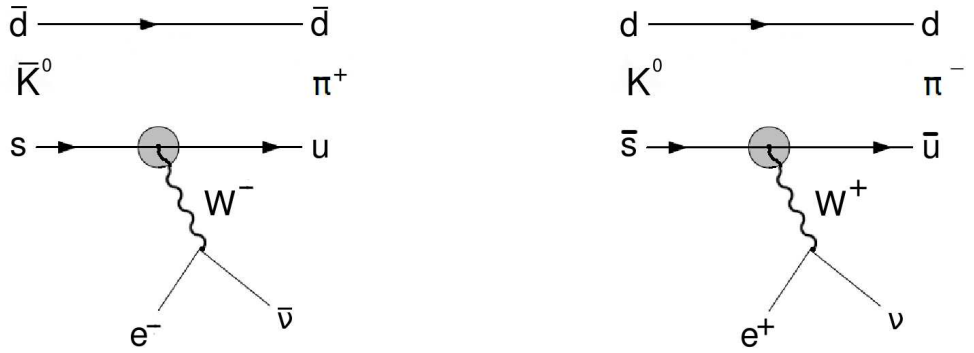

(a) (b)

Figure 2: Feynman diagrams for semileptonic $\bar{K}^0$ (a) and K^0 (b) decays. In the first order, $\bar{K}^0$ can decay to $\pi^+ e^- \bar{\nu}$, but not to $\pi^- e^+ \nu$, and vice versa for K^0.

It will be useful to show that in semileptonic decays neutral kaons obey a $\Delta S = \Delta Q$ rule, where ΔS is the difference of strangeness between final and initial state, and ΔQ is the difference of charge, but only between particles interacting strongly - in this case between a pion and a kaon (obviously, considering the whole reaction, the charge is conserved). This can be explained basing on Feynman diagrams for these processes. Let us consider $\bar{K}^0$ first (Fig. 2a). It consists of two quarks, $\bar{d}$ and s. We assume that quark $\bar{d}$ survives, while quark s decays weakly into quark u by emitting a W^- boson. Then

quarks $\bar{d}$ and u form a positive pion π^+, and W^- decays into $l^-\bar{\nu}$. Note that π^- cannot be created in this decay (at least with the same mechanism). Hence, it is eligible to assume that $\bar{K^0}$ decays into $\pi^+ l^- \nu$, and not into $\pi^- l^+ \nu$. Analogous arguments lead us to the result, that K^0 decays into $\pi^- l^+ \nu$ (corresponding diagram is presented in Fig. 2b).

A common convention is to define amplitudes for semileptonic decays obeying $\Delta S = \Delta Q$ rule as follows:

$$\left\langle \pi^- l^+ \nu \left| T \right| K^0 \right\rangle = a + b, \qquad \left\langle \pi^+ l^- \bar{\nu} \left| T \right| \bar{K^0} \right\rangle = a^* - b^*; \tag{32}$$

and for processes violating $\Delta S = \Delta Q$ rule in a similar way:

$$\left\langle \pi^+ l^- \bar{\nu} \left| T \right| K^0 \right\rangle = c + d, \qquad \left\langle \pi^- l^+ \nu \left| T \right| \bar{K^0} \right\rangle = c^* - d^*. \tag{33}$$

The CPT invariance requires the equality of the probabilities for a kaon and an antikaon to develop into themselves [10]. Hence, a nonzero value of parameter b or d would imply CPT violation. Three new parameters can be introduced:

$$y = -\frac{b}{a}, \qquad x_+ = \frac{c^*}{a}, \qquad x_- = -\frac{d^*}{a}. \tag{34}$$

Parameter y measures CPT violation in processes obeying the $\Delta S = \Delta Q$ rule, whilst x_+ and x_- measure $\Delta S = \Delta Q$ rule violation in processes conserving and violating CPT transformation, respectively. To obtain parameters η_{l^+} and η_{l^-} for semileptonic decays, we first combine eqs. (18), (28), (32) and (33).

$$\begin{aligned}
\left\langle \pi^- l^+ \nu \left| T \right| K_S \right\rangle &= \frac{1}{\sqrt{2\left(1 + \left|\epsilon_S\right|^2\right)}} \left[\left(1 + \epsilon_S\right)(a + b) + \left(1 - \epsilon_S\right)(c^* - d^*) \right], \\
\left\langle \pi^- l^+ \nu \left| T \right| K_L \right\rangle &= \frac{1}{\sqrt{2\left(1 + \left|\epsilon_L\right|^2\right)}} \left[\left(1 + \epsilon_L\right)(a + b) - \left(1 - \epsilon_L\right)(c^* - d^*) \right], \\
\left\langle \pi^+ l^- \bar{\nu} \left| T \right| K_S \right\rangle &= \frac{1}{\sqrt{2\left(1 + \left|\epsilon_S\right|^2\right)}} \left[\left(1 - \epsilon_S\right)(a^* - b^*) + \left(1 + \epsilon_S\right)(c + d) \right], \\
\left\langle \pi^+ l^- \bar{\nu} \left| T \right| K_L \right\rangle &= -\frac{1}{\sqrt{2\left(1 + \left|\epsilon_L\right|^2\right)}} \left[\left(1 - \epsilon_L\right)(a^* - b^*) - \left(1 + \epsilon_L\right)(c + d) \right].
\end{aligned}$$

Let us assume that $\Delta S = \Delta Q$ rule holds. We now calculate parameters η_{l^+} and η_{l^-} for semileptonic decays:

$$\begin{aligned}
\eta_{l^+} &= \frac{\left\langle \pi^- l^+ \nu \left| T \right| K_L \right\rangle}{\left\langle \pi^- l^+ \nu \left| T \right| K_S \right\rangle} = \sqrt{\frac{1 + \left|\epsilon_S\right|^2}{1 + \left|\epsilon_L\right|^2}} \cdot \frac{1 + \epsilon_L}{1 + \epsilon_S} \approx 1 \cdot \left(1 + \epsilon_L\right)\left(1 - \epsilon_S\right) \approx 1 + \epsilon_L - \epsilon_S = 1 - 2\delta, \\
\eta_{l^-} &= \frac{\left\langle \pi^+ l^- \bar{\nu} \left| T \right| K_L \right\rangle}{\left\langle \pi^+ l^- \bar{\nu} \left| T \right| K_S \right\rangle} = -\sqrt{\frac{1 + \left|\epsilon_S\right|^2}{1 + \left|\epsilon_L\right|^2}} \cdot \frac{1 - \epsilon_L}{1 - \epsilon_S} \approx 1 \cdot \left(\epsilon_L - 1\right)\left(1 + \epsilon_S\right) \approx -1 + \epsilon_L - \epsilon_S = -1 - 2\delta.
\end{aligned} \tag{35}$$

For completeness, the general formulae are given by [7]:

$$\begin{aligned}
\eta_{l^+} &= 1 - 2\delta - 2x_+ - 2x_-, \\
\eta_{l^-} &= -1 - 2\delta + 2x_+^* - 2x_-^*.
\end{aligned} \tag{36}$$

The plot of decay intensity for final states $f_1 = \pi^- l^+ \nu$ and $f_2 = \pi^+ l^- \bar{\nu}$ is shown in Fig. 3. The distributions are for $\delta = 0$ (red line) and for $\delta = 5 \cdot 10^{-4} + 0.05i$ (blue line).

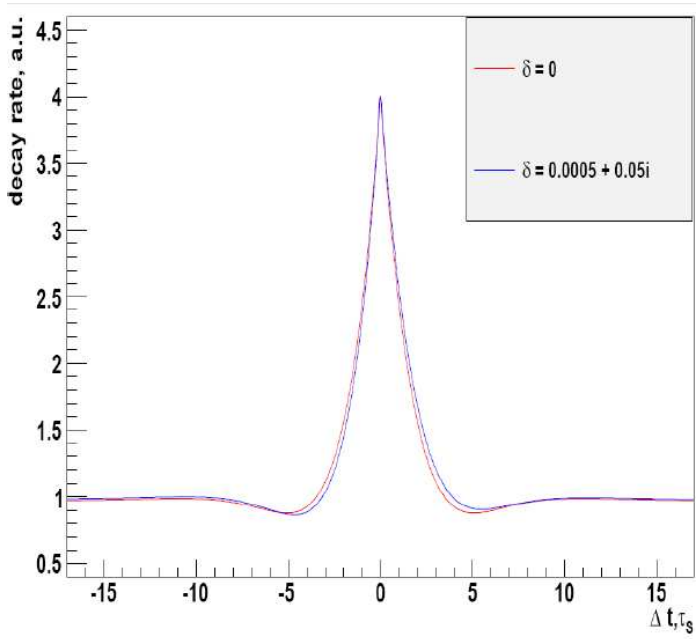

Figure 3: Double decay rate for semileptonic final states with the choice $f_1 = \pi^- l^+ \nu$ and $f_2 = \pi^+ l^- \bar{\nu}$. Red and blue lines correspond to $\delta = 0$ and $\delta = 5 \cdot 10^{-4} + 0.05i$, respectively.

3.3.2 Semileptonic and two pions final state

Having shortly described decays to the same (section 3.2) and similar (3.3.1) final states we proceed to a situation where kaons decay to dissimilar final states, namely to $\pi l \nu$ and $\pi\pi$. From the previous section we know that $|\eta_{l^+}| \approx |\eta_{l^-}| \approx 1$ and from the definition (28) we see that $|\eta_{\pi\pi}|$ is of the order of CP violation, $|\eta_{\pi\pi}| \approx 10^{-3}$ both for $\pi^+\pi^-$ and $\pi^0\pi^0$. Therefore the difference between double decay rates for positive and negative times (29,30) will be of more than five orders of magnitude.

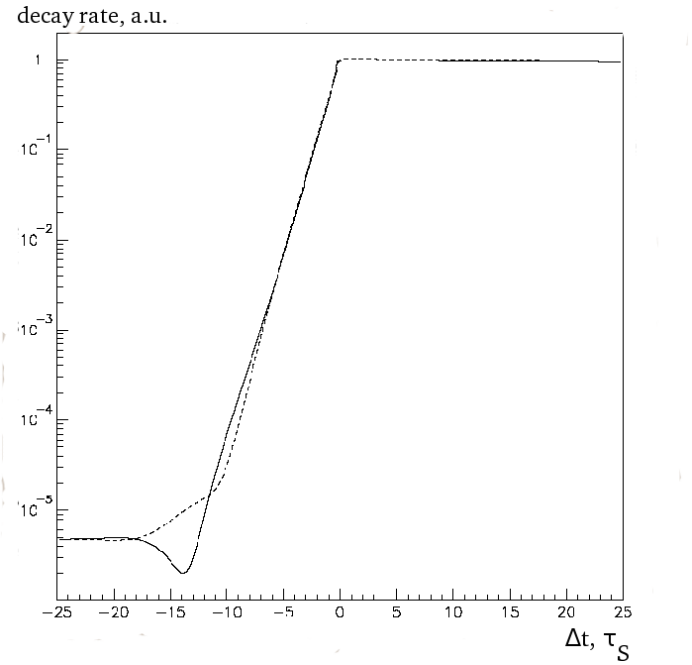

Figure 4: Decay rate intensity $I(\pi l\nu, \pi\pi)$ for $\pi^- l^+ \nu$ (solid line) and $\pi^+ l^- \bar{\nu}$ (dashed line).

Fig. 4 displays the double decay intensity with the choice $f_{1^{\mp}} = \pi^{\pm} l^{\mp} \nu$, $f_2 = \pi\pi$. Interesting pattern can be seen for events in which $\Delta t < 0$. We have:

$$I\left(\pi^{\pm} l^{\mp} \nu, \pi\pi; \Delta t < 0\right) = \frac{C_{1^{\mp}2}}{\Gamma_S + \Gamma_L} \Big\{ |\mp 1 - 2\delta|^2 \, e^{-\Gamma_S |\Delta t|} + |\eta_{\pi\pi}|^2 \, e^{-\Gamma_L |\Delta t|} + \\ - 2\,|\mp 1 - 2\delta| \, |\eta_{\pi\pi}| \, e^{-\frac{\Gamma_L + \Gamma_S}{2} |\Delta t|} \cos\left[\Delta m \, |\Delta t| + \phi_{\pi l \nu} - \phi_{\pi\pi}\right] \Big\} . \tag{37}$$

We note that the right-hand side of the equation above has three terms corresponding to three regions in Fig. 4. For small negative Δt eq. (37) is dominated by the first term, which decays rapidly as $e^{-\Gamma_S |\Delta t|}$, then there is interference region with its term involving $|\eta_{\pi\pi}|$, Δm and $\phi_{\pi\pi}$, and finally the second term results in K_L decay shape suppressed by $|\eta_{\pi\pi}|^2$ for $\Delta t < 20\tau_S$. Therefore from measuring distributions with the final states considered we can gain knowledge about phases ϕ_{+-} and ϕ_{00}, absolute values of η_{+-} and η_{00} parameters and mass difference $\Delta m = m_L - m_S$. However, more precise value of Δm can be extracted from measuring $(\pi^+\pi^-, \pi^+\pi^-)$ final states, while for $|\eta_{+-}|$ and $|\eta_{00}|$ more accurate results may be obtained from analysing inclusive $\pi\pi$ distributions [13].

4 Connection between double decay rate and CPT symmetry

4.1 Quantum entanglement, EPR paradox

As already described in section 3.2, considering the double decay rate to identical final states, according to quantum mechanics we do not expect any events in $\Delta t = 0$. This is very counterintuitive, as the two decays are space-like separated events and one could think that each kaon should behave independently of the other one. This kind of correlation is of the type first mentioned by Einstein, Podolsky and Rosen in their well-known article [14], where the authors criticize Bohr's view of quantum mechanics and, basing on a thought-experiment whose outcome is not only nonintuitive, but also appears to be nonlocal, suggest that quantum-mechanical description of physical reality given by wave functions cannot be considered complete. This type of connection between particles was soon investigated further by Schrödinger, who coined a term entanglement (Verschränkung) to describe the perplexing bond between quantum systems [15]. Obviously Schrödinger could not have known about kaons at the time of writing his paper, instead he considered a two-body decay and the measurement of positions and momenta of particles in view of Pauli exclusion principle. An interested reader is also referred to Ref. [16].

The term decoherence in general means the time evolution of a pure state into an incoherent mixture of states [7]. To account for possible decoherence in the neutral kaons system phenomenologically, one can simply modify the equation for the double decay rate (26) by multiplying the interference term by a factor $(1-\zeta)$, where ζ is a decoherence parameter:

$$\begin{aligned} I(f_1,t_1;f_2,t_2) = C_{12}\{&|\eta_1|^2 e^{-\Gamma_L t_1-\Gamma_S t_2} + |\eta_2|^2 e^{-\Gamma_S t_1-\Gamma_L t_2} + \\ &- 2(1-\zeta)|\eta_1||\eta_2| e^{-\frac{\Gamma_S+\Gamma_L}{2}(t_1-t_2)}\cos\left[\Delta m (t_1-t_2)+\phi_2-\phi_1\right]\}. \end{aligned} \tag{38}$$

By taking $\zeta = 0$ eq. (26) is recreated (so it is quantum mechanics case), while the case of $\zeta = 1$ corresponds to total decoherence. As it turns out, the parameter ζ is basis-dependent [17]. Current measurements of ζ in the two main bases, $\{|K_S\rangle, |K_L\rangle\}$ and $\{|K^0\rangle, |\bar{K}^0\rangle\}$, are compatible with no deviations from quantum mechanics [18]:

$$\begin{aligned} \zeta_{SL} &= \left(0.3 \pm 1.8_{\text{stat}} \pm 0.6_{\text{syst}}\right) \cdot 10^{-2}, \\ \zeta_{0\bar{0}} &= \left(1.4 \pm 9.5_{\text{stat}} \pm 3.8_{\text{syst}}\right) \cdot 10^{-7}. \end{aligned} \tag{39}$$

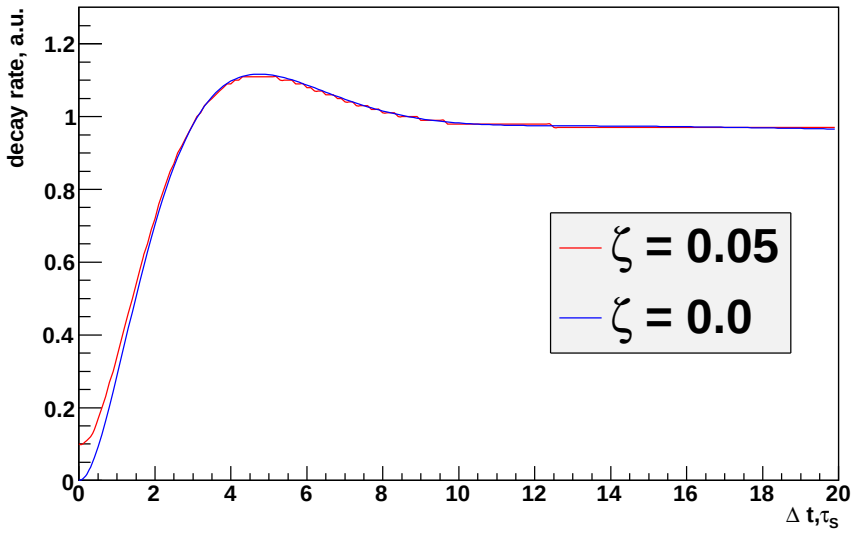

Figure 5: Decay rate as a function of Δt for eq. (38). The blue and red lines are for $\zeta = 0$ and $\zeta = 0.05$ respectively. The biggest discrepancy between these two functions is for Δt close to 0.

Fig. 5 illustrates the difference between the double decay rates for two values of ζ_{SL}: $\zeta_{SL} = 0$ and $\zeta_{SL} = 0.05$. From these plots one concludes that nonzero ζ_{SL} parameter would manifest itself mainly in the region close to $\Delta t = 0$.

4.2 Evolution of pure into mixed states

A discussion of a new source of CPT and quantum mechanics violation was opened when Hawking showed that black holes can create particles and evaporate by emitting them, resembling hot bodies [19]. In his subsequent papers [20] he introduced the idea of the evolution of pure states into mixed states in the vicinity of black holes. Assume one started from an initial pure quantum state (described in terms of a complete set of commuting observables), which would partially fall through the event horizon inside the black hole. The description of this quantum state in terms of observables in the future would require two sets of observables, observables at infinity describing outgoing particles, and observables inside the black hole describing what fell through the event horizon. As one even in principle cannot measure what fell into a black hole, the observation would have to be described by a mixed state obtained by summing over all possible black hole states. This is in contradiction with quantum mechanics, where a pure state remains pure through its evolution and is forbidden to evolve into a mixed one. Moreover, according to proof by Wald [21], such evolution from pure to mixed states is incompatible with T or CPT invariance. Hawking further predicts that the most probable scenario for a black hole is its complete disappearance accompanied by the loss of information about its states, and argues that such transitions from pure into mixed states are also possible on a microscopic (elementary particle) level because of quantum fluctuations of the metric, which could be interpreted as virtual black holes which appear and disappear again.

Theoretical considerations described above led Ellis *et al.* to develop an appropriate phenomenological framework for discussing violations of quantum mechanics due to evolution of pure states into mixed states [22]. The formalism introduced is applied to neutron interferometry and to experiments involving neutral kaons, on which we will concentrate. In general, the approach is based on density matrix rather than on Hamiltonian equation. Let $\mathbf{H}$ be the Hamiltonian defined in eq. (5) and ρ the density matrix. The following modification of Liouville-von Neumann equation is proposed (here a slightly simplified notation from Ref. [7] is used):

$$\frac{d\rho}{dt} = -i\mathbf{H}\rho + i\rho\mathbf{H}^\dagger + i\delta\not{\mathbf{H}}\rho \tag{40}$$

The last term on the right-hand side of the above equation is responsible for decoherence. When one expands ρ in terms of Pauli spin matrices σ_i and the identity σ_0 and uses the basis of CP eigenstates for kaons, $\delta\not{\mathbf{H}}$ can be represented by a 4×4 matrix $\delta\not{H}_{\mu\nu}$ which acts on a column vector with ρ_μ as components. The elements of $\delta\not{\mathbf{H}}$ should respect two natural restrictions, namely they ought to be consistent with probability conservation and they should not decrease the entropy of the system (in other words, mixed states should not be allowed to evolve into pure states). The authors of Ref. [22] added a condition that the new term cannot change strangeness. Taking into account these constraints, the $\delta\not{\mathbf{H}}$ matrix is found to have only four non-vanishing elements:

$$\delta\not{\mathbf{H}} = -2\begin{pmatrix} 0 & 0 & 0 & 0 \\ 0 & 0 & 0 & 0 \\ 0 & 0 & \alpha & \beta \\ 0 & 0 & \beta & \gamma \end{pmatrix}. \tag{41}$$

Here α, β and γ are three real parameters violating CPT and quantum mechanics. To ensure that $\mathrm{Tr}\rho^2$ does not exceed unity (so that we avoid states with complex entropy), they should satisfy the inequalities $\alpha > 0$, $\gamma > 0$ and $\alpha\gamma > \beta^2$ [22]. See also section 6.3 for expected boundaries of their values.

The extension of this formalism to a pair of entangled kaons was done by Huet and Peskin [23]. Among other results, they obtained the double decay rate in terms of decay times t_1, t_2 and α, β, γ

parameters for the decay to $(\pi^+\pi^-;\pi^+\pi^-)$:

$$
\begin{aligned}
&I\left(\pi^+\pi^-,t_1\ ;\ \pi^+\pi^-,t_2\right) = \\
&\quad = 2\left|A_0\right|^4\Big\{R_L\left(e^{-\Gamma_S t_1-\Gamma_L t_2}+e^{-\Gamma_L t_1-\Gamma_S t_2}\right)-2\left|\bar{\eta}_{+-}\right|^2\cos\left[\Delta m\left(t_1-t_2\right)\right]e^{-\left(\bar{\Gamma}+\alpha-\gamma\right)(t_1+t_2)} \\
&\qquad + 4\frac{\beta}{|d|}\left|\bar{\eta}_{+-}\right|\sin\left(\Delta m t_1+\phi_{+-}-\phi_{SW}\right)e^{-\left(\bar{\Gamma}+\alpha-\gamma\right)t_1}e^{-\Gamma_S t_2}+ \\
&\qquad + 4\frac{\beta}{|d|}\left|\bar{\eta}_{+-}\right|\sin\left(\Delta m t_2+\phi_{+-}-\phi_{SW}\right)e^{-\left(\bar{\Gamma}+\alpha-\gamma\right)t_2}e^{-\Gamma_S t_1}+ \\
&\qquad - 2\left(\frac{\gamma}{\Delta\Gamma}+2\frac{\beta}{|d|}\left|\bar{\eta}_{+-}\right|\frac{\sin\phi_{+-}}{\cos\phi_{SW}}\right)e^{-\Gamma_S(t_1+t_2)}\Big\},
\end{aligned}
\tag{42}
$$

where:

$d=\Delta m+\frac{i}{2}\Delta\Gamma$ (Δm and $\Delta\Gamma$ are defined to be positive, i.e. $\Delta m=m_L-m_S$ and $\Delta\Gamma=\Gamma_S-\Gamma_L$),

$|\bar{\eta}_{+-}|e^{i\phi_{+-}}=\epsilon_L^-$,

$\epsilon_L^-=\epsilon_L-\frac{\beta}{d}$,

$R_L=|\epsilon_L^-|^2+\frac{\gamma}{\Delta\Gamma}+\frac{4\beta}{\Delta\Gamma}\Im\left(\frac{\epsilon_L^- d}{d^*}\right)$.

Now we repeat the procedure described in section 3.1, i.e. a switch to $t=t_1+t_2$ and $\Delta t=t_1-t_2$ variables followed by integration in t. Since the final states in this case are identical, it is enough to calculate the double decay rate for $\Delta t\geq 0$. The result is:

$$
\begin{aligned}
&I\left(\pi^+\pi^-,\pi^+\pi^-\ ;\Delta t\right) = \\
&\quad = \left|A_0\right|^4\left|\bar{\eta}_{+-}\right|^2\Big\{\frac{R_L}{\left|\bar{\eta}_{+-}\right|^2\cdot\bar{\Gamma}}\left(e^{-\Gamma_S\Delta t}+e^{-\Gamma_L\Delta t}\right)-\frac{2}{\bar{\Gamma}+\alpha-\gamma}\cos\left(\Delta m\Delta t\right)e^{-\left(\bar{\Gamma}+\alpha-\gamma\right)\Delta t}+ \\
&\qquad + \frac{8\beta}{|d|\left|\bar{\eta}_{+-}\right|\left[\left(\bar{\Gamma}+\alpha-\gamma+\Gamma_S\right)^2+\left(\Delta m\right)^2\right]}\cdot \\
&\qquad \cdot\Big[\left[\left(\bar{\Gamma}+\alpha-\gamma+\Gamma_S\right)\sin\left(\Delta m\Delta t+\phi_{+-}-\phi_{SW}\right)+\Delta m\cos\left(\Delta m\Delta t+\phi_{+-}-\phi_{SW}\right)\right]e^{-\left(\bar{\Gamma}+\alpha-\gamma\right)\Delta t}+ \\
&\qquad + \left[\left(\bar{\Gamma}+\alpha-\gamma+\Gamma_S\right)\sin\left(\phi_{+-}-\phi_{SW}\right)+\Delta m\cos\left(\phi_{+-}-\phi_{SW}\right)\right]e^{-\Gamma_S\Delta t}\Big]+ \\
&\qquad - \frac{2}{\Gamma_S}\left(\frac{\gamma}{\Delta\Gamma\left|\bar{\eta}_{+-}\right|^2}+\frac{2\beta}{|d|\left|\bar{\eta}_{+-}\right|}\frac{\sin\phi_{+-}}{\cos\phi_{SW}}\right)e^{-\Gamma_S\Delta t}\Big\}.
\end{aligned}
\tag{43}
$$

5 KLOE and KLOE-2 experiments

The K Long Experiment (KLOE) [24, 25, 26], which started data taking in 1999 and concluded in 2006, was located at the crossing point of electron and positron beams of DAΦNE collider [27] at Laboratori Nazionali di Frascati (LNF) in Frascati, Italy. Now, in the year 2010, a new experiment - KLOE-2 [28] - is about to start at the same place. When compared to its predecessor, the main changes in the new experiment are a new collision scheme of DAΦNE collider and additional detectors - inner tracker, calorimeters and $\gamma\gamma$ taggers. In this chapter DAΦNE collider is described (5.1), then KLOE detector components: drift chamber (5.2.1) and electromagnetic calorimeter (5.2.2) are introduced. Finally new detectors involved in KLOE-2 experiment are briefly discussed (5.3)

5.1 DAΦNE collider

DAΦNE (Double Annular Φ-factory for Nice Experiments) is an electron-positron collider. As the name suggests, most of the time it operates with a centre of mass energy around the ϕ meson mass, $M_\phi = (1019.455 \pm 0.020)$ MeV. The ϕ production cross-section is large and peaks at about 3 microbarns. Due to high luminosity and the fact that ϕ mesons decay predominantly to kaon pairs (charged and neutral, see Tab. 2), the ϕ-factory is especially suitable for investigations in the field of kaon physics. The components of DAΦNE are a 60 m long linear accelerator (LINAC), a 32 m long accumulator and two 100 m long main rings. The layout of the DAΦNE facility is presented in Fig. 6.

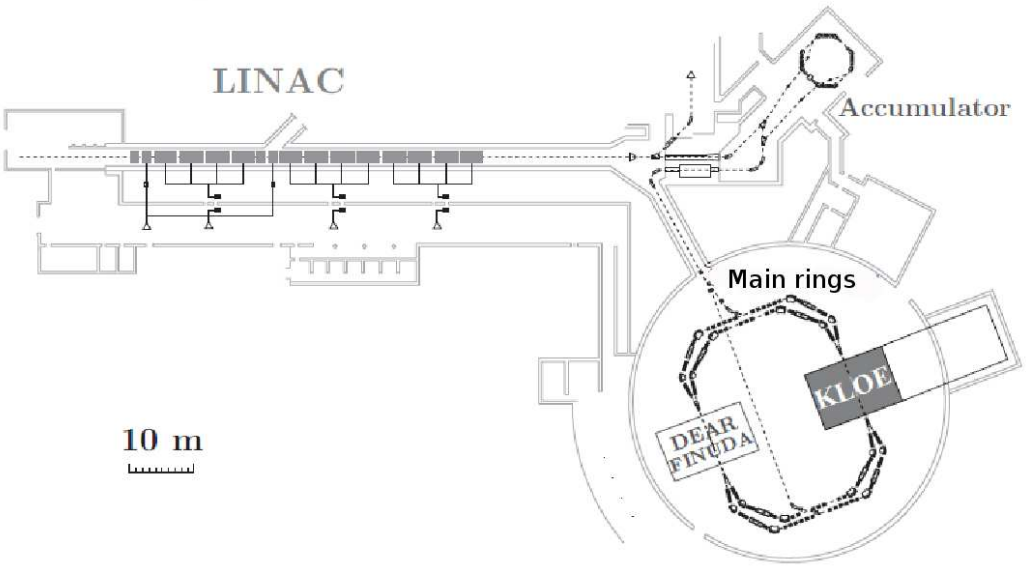

Figure 6: DAΦNE facility layout. The figure is adapted from [25].

LINAC can work in two modes, alternately producing and accelerating electron and positron beams to energies of 510 MeV (about half of the ϕ meson mass). Once produced and accumulated, electrons and positrons circulate in two separate rings to reduce beam-beam interaction. Particles are formed into bunches, and most of the time the number of particles in a bunch is kept on the level of 10^{10}, although this number can be smaller for a given bunch. There are up to 120 bunches in each ring. In KLOE experiment every bunch collided with its counterpart from the other ring in one of two interaction regions (see Fig. 7). The other interaction region was used for other experiments conducted at LNF - FINUDA and DEAR. The situation is different for KLOE-2, as there is going to be only one region where the beams cross. Selected parameters of DAΦNE can be found in Table 3.

Table 3: DAΦNE selected parameters.

Parameter	Value
Energy of particles	510 MeV
Number of bunches	up to 120 per ring
Number of particles in a bunch	$\sim 10^{10}$
Frequency of collisions	$\sim$ 370 MHz

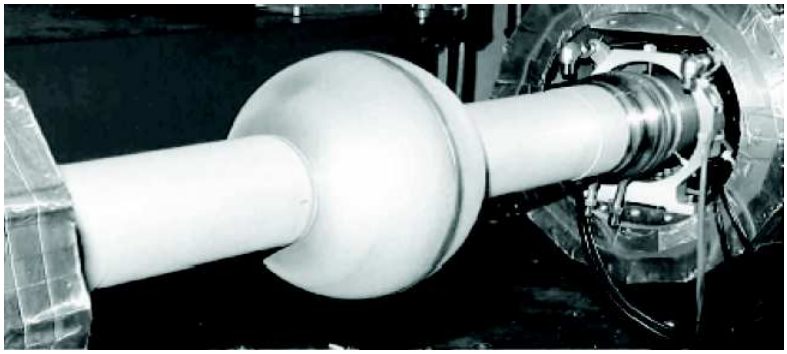

Figure 7: A fragment of the beam pipe surrounding the KLOE interaction region. The figure is adapted from [29].

5.2 Detectors

KLOE detection system has already been described in details in many publications - an interested reader is referred to, for instance, Ref. [24] and [25]. Here only essential components of the detector - drift chamber and electromagnetic calorimeter - are briefly reviewed. A schematic view of KLOE is given in Fig. 8.

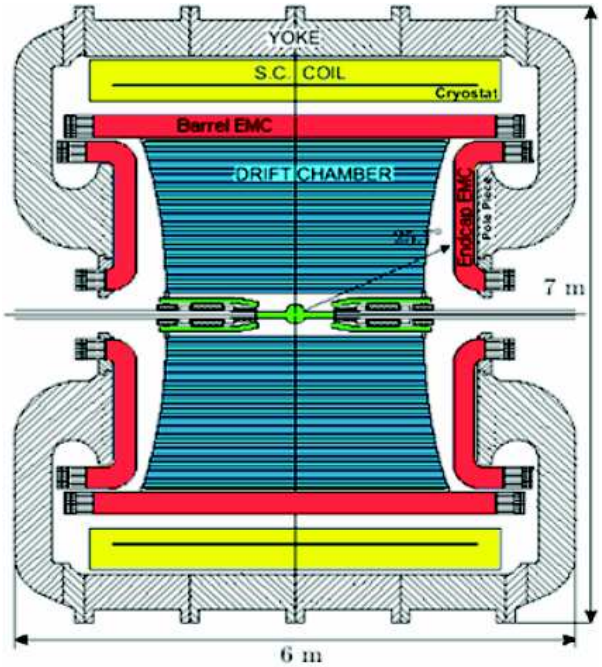

Figure 8: KLOE cross-section. The main components are the drift chamber and electromagnetic calorimeter (EMC), surrounded by a superconducting coil. The figure is adapted from [30].

5.2.1 Drift Chamber

The design of the drift chamber (see Fig. 9) was driven by the desire to observe kaons' decay products from the $\phi \rightarrow K^0\bar{K}^0$ reactions. To accomplish this goal, it was needed to take into account a relatively long lifetime of K_L, $\tau_L \approx 51$ ns (for this and more features of K_L and K_S, refer to Tab. 1). Knowing that kaons are produced with momenta ~ 115 MeV/c, the mean path travelled by a K_L meson is readily obtained as $\lambda_L = \beta\gamma c\tau_L \approx 3.5$ m (the mean path of K_S, computed in the same way, is $\lambda_S \approx 5.6$ mm). The solution applied is a cylindrical drift chamber, whose diameter and maximal length are 4 m and 3.3 m respectively (the inner radius is 25 cm). This volume allows us to catch about 30 - 40% of K_L decays.

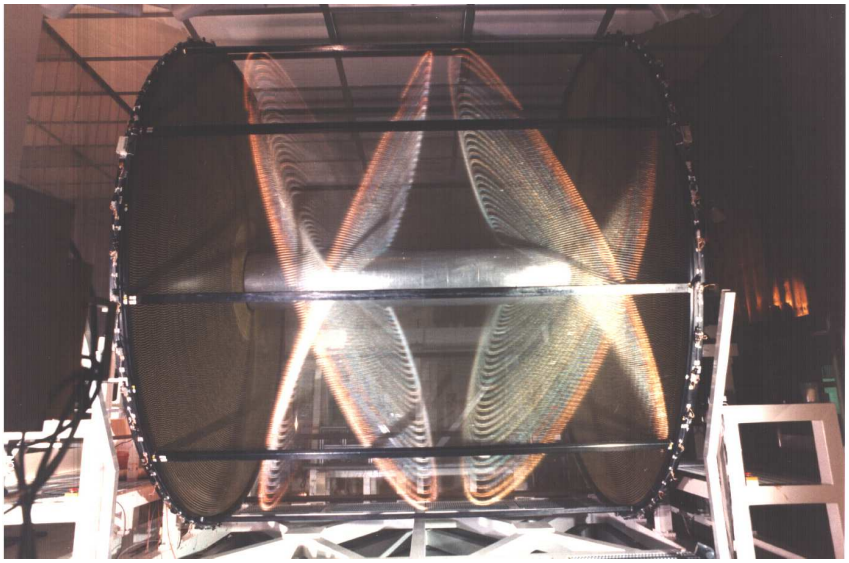

Figure 9: KLOE drift chamber after completing the assembly. Light reflection on wires can be seen. The figure is adapted from [26].

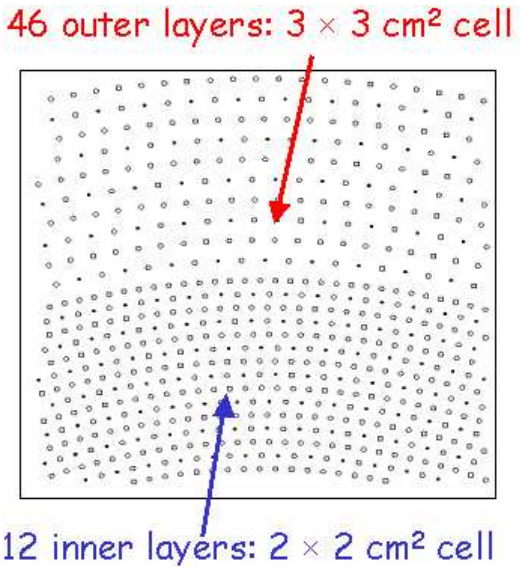

Figure 10: Cells configuration of the KLOE drift chamber. Full points indicate sense wires, while points empty inside show field wires. The figure is adapted from [26].

Another important requirement for the drift chamber [26] is that it has a high and uniform reconstruction efficiency over a large volume. Moreover, it is demanded to have a good momentum resolution. To meet this criteria, a uniform structure of drift cells ensuring high homogeneity over the whole volume was planned. To achieve this, the drift chamber was filled with 58 coaxial layers of wires, giving a total of 12582 almost square cells (each with one sense wire). Altogether there are over 50 thousands of wires, the ratio of the field to sense wires being 3:1. Since the track density is much higher at small radii due to the relatively small momenta of particles produced in the ϕ meson decays [31], and because reconstructing K_S mesons vertices is desired, 12 innermost layers have cells of smaller size, 2 cm x 2 cm, while the cells of 46 outermost layers are of the size 3 cm x 3 cm. Configuration of the drift cells is presented in Fig. 10. Wires belonging to the same layer are parallel to each other, while each layer is slightly twisted with respect to the neighbouring ones. It turns out that the drift chamber is able to measure charged vertices of K_S and K_L with $\sim$ 1 mm accuracy and provides fractional momentum resolution of $\frac{\sigma_p}{p} \sim 0.5\%$ [32].

One more feature demanded from the drift chamber, especially important for neutral kaons physics, is its transparency to particles in order to minimize K_L into K_S regeneration, multiple scattering and conversion of low energy photons. For this reason, low-atomic-number materials were chosen: carbon fiber composite for the mechanical structure, and the mixture of 90% helium - 10% isobutane for the drift medium. Taking into account also the presence of wires, the average radiation length in the whole chamber volume is estimated to be about $X_0^{\mathrm{DC}} \sim 900$ m [33].

5.2.2 Electromagnetic calorimeter

There is a number of requirements that are expected from KLOE electromagnetic calorimeter (Fig. 11). To start with, basing on the time measurement of the arrival of neutral decay products

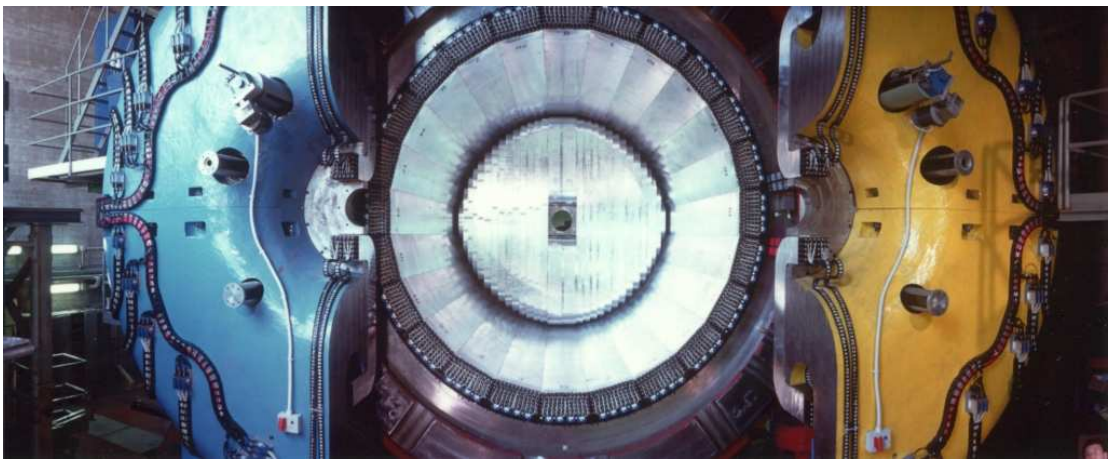

Figure 11: Electromagnetic calorimeter of KLOE. The figure is adapted from [26].

of kaons, it should allow to determine K_S and K_L neutral vertices with an accuracy of few milimeters. As the flight path of K_L before it decays into neutral pions is calculated basing on the time of arrival of the photons from π^0 decays, a good time resolution is necessary (with a precision of 100 ps, the flight path is determined to $\sim$ 0.6 cm [34]). Another task of the calorimeter is to distinguish CP-violating $K_L \to 2\pi^0$ from $K_L \to 3\pi^0$ decay. For this reason, the calorimeter should cover as much of the 4π angle as possible and the effects of splitting and merging of signals should be minimised. To reach this goals, a calorimeter consisting of a cylindrical, central barrel and two endcaps was built, all of them marked red in Fig. 8. As a result, 98% of the 4π angle is covered. The barrel consists of 24 modules of trapezoidal shape, each 23 cm thick (which corresponds to about $15X_0$ [30]), whilst each endcap consists of 32 vertical modules, which are bent on both sides into a C-shape. The length of these modules varies from 70 cm to 3.9 m. Particles crossing the electromagnetic calorimeter are detected as local energy

deposits. When the deposits are close in time and space, they are grouped into clusters. Energy and time resolutions for electromagnetic showers are [35]:

$$\frac{\sigma(E)}{E} = \frac{5,7\%}{\sqrt{E(\mathrm{GeV})}}, \qquad \sigma(t) = \frac{57 \text{ ps}}{\sqrt{E(\mathrm{GeV})}} \oplus 100 \text{ ps}.$$

5.3 KLOE-2 upgrades

As already mentioned, in KLOE-2 experiment several new detectors are going to be used. In this section a short description of these new elements is provided. Fig. 12 illustrates the positions of the inner tracker and electromagnetic calorimeters (CCALs and QCALs).

5.3.1 Inner tracker

Without doubt this is the most important upgrade when kaon physics is considered. It is expected to increase the geometrical acceptance for low momentum tracks, as well as to improve effectiveness of the decay vertex reconstruction and the track momentum resolution by reducing the track extrapolation length [35].

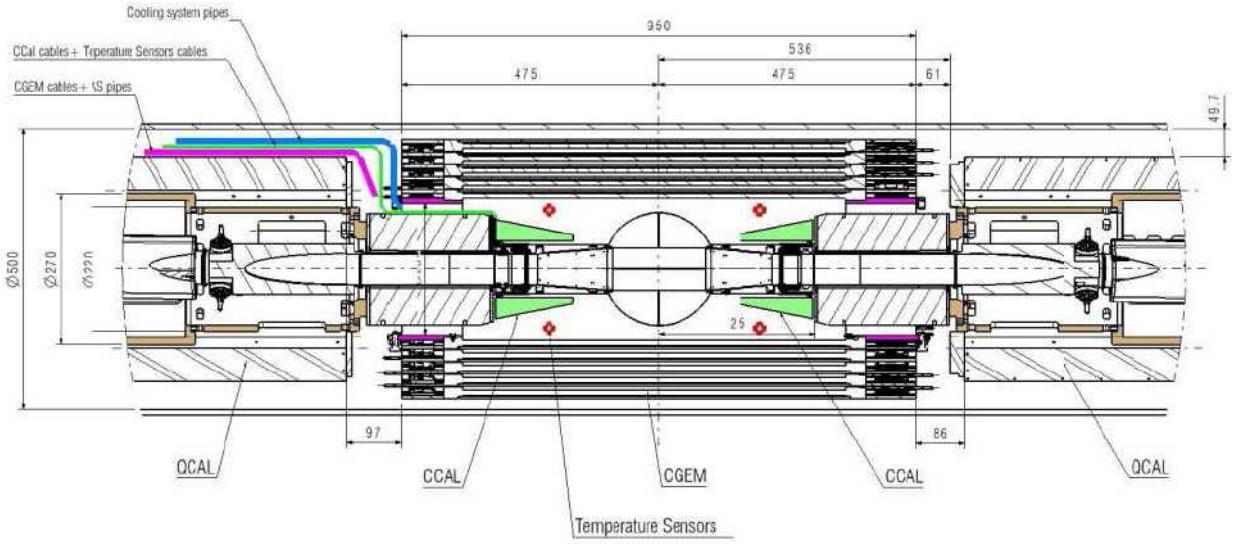

Figure 12: KLOE-2 detector scheme around the interaction point. CGEM denotes cylindrical gas electron multipliers, CCAL stands for crystal calorimeters, and QCAL indicates quadrupole tile calorimeters. The figure is adapted from [36].

The inner tracker will consist of four cylindrical GEM (CGEM) detectors (GEM standing for gas electron multiplier, detector described for the first time in Ref. [37]). It will be about 50 cm long, placed between the beam pipe and the drift chamber inner wall. While the radius of the outermost layer is naturally limited by the presence of the drift chamber, the radius of the innermost layer should be chosen in order not to destroy the interference pattern (for example in Fig. 1) due to K_S regeneration phenomenon. Taking into account these constrains, inner and outer radii of the inner tracker have been designed to be 129.5 mm and 220 mm, respectively [36]. 129.5 mm corresponds to about $23\tau_S$, so, as can be deduced from Fig. 1, the interference pattern will not be destroyed. Simulations results [38] indicate that thanks to this detector the uncertainty of the vertex position can be reduced by a factor $\sim$2.5.

5.3.2 Calorimeters

The motivation for using extra calorimeters (apart from the barrel and endcaps described in 5.2.2) is to increase the detector acceptance for photons coming from the vicinity of the interaction region. Important analyses which can benefit from these detectors include the search for $K_S \to 3\pi^0$ decay and measurements of $K_S \to \gamma\gamma$ and $\eta \to \pi^0\gamma\gamma$ branching ratios [39]. Two types of calorimeters are going to be used:

- CCALT [40, 41, 42] - crystal calorimeters with timing, located between the end of the spherical beam pipe (of 10 cm radius) and the first quadrupole (30 cm from the interaction point). These detectors will extend the angular coverage of the KLOE-2 electromagnetic calorimeter from polar angle of 20° down to 8°. Each of them will consist of two concentrical, cylindrical barrels. The material used is cerium-doped LYSO ($Lu_{18}Y_{0.2}SiO_5 : Ce$). When compared to $PbWO_4$, its scintillation emission time is 4 times longer, but it is more than compensated for by 300 times larger light yield.
- QCALT [40, 41, 43] - quadrupole tile calorimeters sorrounding the inner quadrupoles. As QCALTs should improve the reconstruction of $K_L \to 2\pi^0$ decays, there is a number of features required from these detectors, including high efficiency to low energy (20-300 MeV) photons, time resolution of less than 1 ns and space resolution of few centimeters. QCALTs are 1 m long with dodecagonal structure and they are composed of five 5 mm thick scintillator plates alternated with 3.5 mm thick tungsten plates, together giving a depth of 5.5 X_0.

5.3.3 $\gamma\gamma$ taggers

The goal of using $\gamma\gamma$ taggers is, as the name suggests, to tag the presence of a pair of photons in the drift chamber. To achieve this goal, it is necessary to measure electrons (positrons), whose energy is lower than nominal 510 MeV. From such measurement one infers that e^+ and e^- interacted, and it is assumed that the reaction was of the form $e^+e^- \to e^+e^-\gamma^*\gamma^* \to e^+e^-X$.

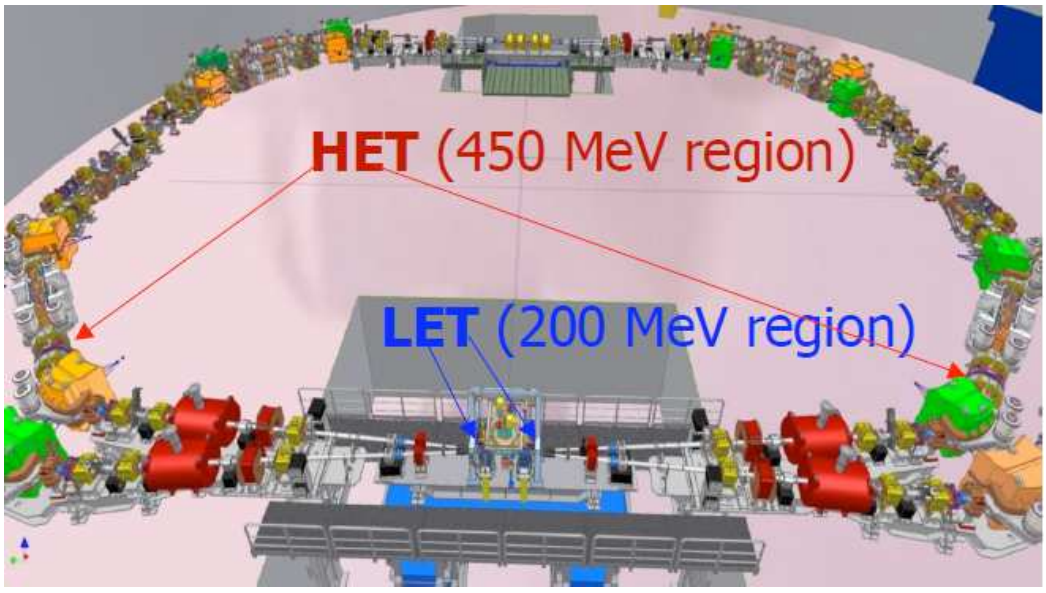

Figure 13: Positions of $\gamma\gamma$-tagging detectors. Positions of Low Energy Tagger (LET) and High Energy Tagger (HET) are indicated by arrows. The figure is adapted from [44].

Simulation shows that electrons with energies below 250 MeV will exit the beam pipe within 1 m from the interaction point [45], while those with energies greater than 420 MeV, focused by the first

focusing quadrupole, will leave the vacuum chamber downstream the bending magnet [39]. The detectors measuring low- and high-energy electrons are called LET (standing for low energy tagger) and HET (high energy tagger), respectively, and their positions are shown in Fig. 13 (note that 'low' and 'high' here actually apply to the measured electrons, not to tagged photons). For particles reaching HET there is a clear correlation between energy and position, hence a position-sensitive detector can be used [46]. On the other hand particles detected in LET show no such correlation, and for this reason LET has to be an energy-sensitive detector, i.e. a calorimeter [45].

6 Function $I(\pi^+\pi^-,\pi^+\pi^-\ ;\Delta t)$ with parameters α,β,γ - fit to data

In this chapter the results of fitting the function (43) to the experimental data are reported. The cuts used in the data analysis are listed in section 6.1, further technical information is provided in section 6.2. Finally, in 6.3, obtained results are compared to previous measurements published by KLOE and CPLEAR collaborations.

6.1 Cuts applied

The following cuts were applied to the preselected [47] data set before making the fit:

- on K_L invariant mass:

$$\sqrt{2\left(m_\pi^2+\sqrt{\left(m_\pi^2+\vec{p}_{\pi_1}^{\,2}\right)\left(m_\pi^2+\vec{p}_{\pi_2}^{\,2}\right)}-\sum_{i=x,y,z}p^i_{\pi_1}p^i_{\pi_2}\right)}-m_{K^0}<5\ \text{MeV}$$

- on K_S and K_L missing masses:

$$10\ \text{MeV}^2>\sum_{i=x,y,z}\left[\left(\sqrt{m_{K^0}^2+\left(p^i_{K_{S(L)}}\right)^2}-\sqrt{m_\pi^2+\left(p^i_{\pi_{1S(L)}}\right)^2}-\sqrt{m_\pi^2+\left(p^i_{\pi_{2S(L)}}\right)^2}\right)^2+\right.$$
$$\left.-\left(p^i_{K_{S(L)}}-p^i_{\pi_{1S(L)}}-p^i_{\pi_{2S(L)}}\right)^2\right]>-50\ \text{MeV}^2$$

- on K_S and K_L missing momenta:

$$\sqrt{\sum_{i=x,y,z}\left(p^i_{K_{S(L)}}-p^i_{\pi_{1S(L)}}-p^i_{\pi_{2S(L)}}\right)^2}<10\ \text{MeV}$$

- on event global fit:

$$\sum_{\substack{K=K^0,\bar{K}^0\\ i=x,y,z}}\left(\frac{V_i^K-\left(V_i^\phi+l^K\hat{n}_i^K\right)}{\sigma_i}\right)^2<15,$$

where (see also Fig. 14):
V_i^K- ith component of a kaon's vertex position,
$V_i^\phi-$ ϕ decay position along the ith axis,
l^K- kaon's decay length,
$\hat{n}_i^K-$ kaon's direction obtained from reconstructed tracks,
σ_i- uncertainty of the kaon's decay vertex (quantity derived from Monte Carlo).

6.2 Assumptions

6.2.1 Fitting function

The fitting function is of the form:

$$n_i=N\left(\sum_j s_{ij}\epsilon_j I_j\left(\alpha,\beta,\gamma\right)\right)\ , \tag{44}$$

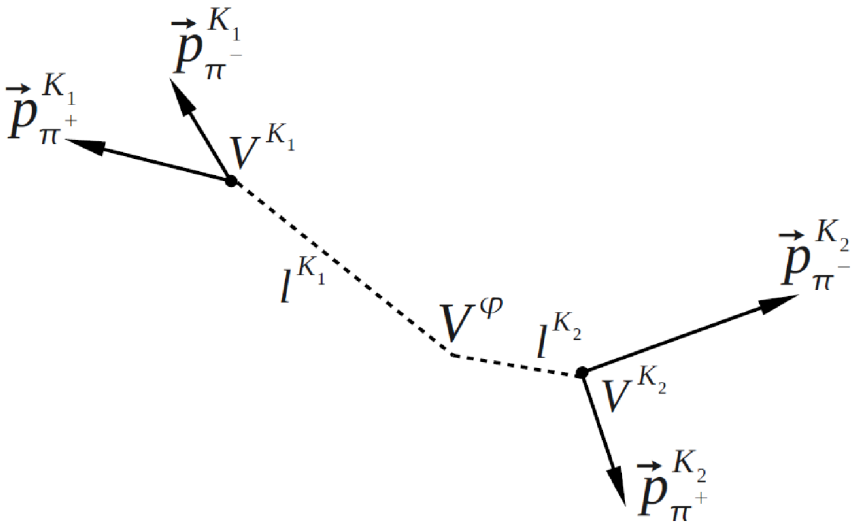

Figure 14: Pictorial definition of variables in the event global fit. The figure is adapted from [48].

where n_i is the expected number of events in the ith bin, N is the normalizing factor (the number of $K_S K_L \to \pi^+\pi^-\pi^+\pi^-$ events), s_{ij} and ϵ_j are the smearing matrix and efficiency vector, and finally I_j is the function (43) integrated over the bin width of the data histogram:

$$I_{t'}(\alpha,\beta,\gamma) = \int_{t'}^{t'+\delta t'} I\left(\pi^+\pi^-,\pi^+\pi^-\,;\Delta t\right) d(\Delta t)\ . \tag{45}$$

Let us define $\Delta\phi := \phi_{+-} - \phi_{SW}$. Then the result of (45) is:

$$\begin{aligned}
&I_{t'}(\alpha,\beta,\gamma) = \\
&= |A_0|^4 |\bar{\eta}_{+-}|^2 \left\{ \frac{R_L}{|\bar{\eta}_{+-}|^2 \bar{\Gamma}} \left[\frac{1}{\Gamma_S}\left(e^{-\Gamma_S t'} - e^{-\Gamma_S(t'+\delta t')}\right) + \frac{1}{\Gamma_L}\left(e^{-\Gamma_L t'} - e^{-\Gamma_L(t'+\delta t')}\right)\right] + \right. \\
&\quad - \frac{2}{\left(\bar{\Gamma}+\alpha-\gamma\right)\left[\left(\bar{\Gamma}+\alpha-\gamma\right)^2 + (\Delta m)^2\right]} \cdot \\
&\quad \cdot \left[e^{-\left(\bar{\Gamma}+\alpha-\gamma\right)(t'+\delta t')} \left(\Delta m \sin\left(\Delta m\left(t'+\delta t'\right)\right) - \left(\bar{\Gamma}+\alpha-\gamma\right)\cos\left(\Delta m\left(t'+\delta t'\right)\right)\right) + \right. \\
&\quad \left. - e^{-\left(\bar{\Gamma}+\alpha-\gamma\right)t'} \left(\Delta m \sin\left(\Delta m t'\right) - \left(\bar{\Gamma}+\alpha-\gamma\right)\cos\left(\Delta m t'\right)\right)\right] + \\
&\quad + \frac{8\beta}{|d|\,|\bar{\eta}_{+-}| \left[\left(\bar{\Gamma}+\alpha-\gamma+\Gamma_S\right)^2 + (\Delta m)^2\right]\left[\left(\bar{\Gamma}+\alpha-\gamma\right)^2 + (\Delta m)^2\right]} \cdot \\
&\quad \cdot \left\{ \left(\bar{\Gamma}+\alpha-\gamma+\Gamma_S\right) \left\{ e^{-\left(\bar{\Gamma}+\alpha-\gamma\right)t'} \left[\left(\bar{\Gamma}+\alpha-\gamma\right)\sin\left(\Delta m t'+\Delta\phi\right) + \Delta m \cos\left(\Delta m t'+\Delta\phi\right)\right] + \right.\right. \\
&\quad \left. - e^{-\left(\bar{\Gamma}+\alpha-\gamma\right)(t'+\delta t')} \left[\left(\bar{\Gamma}+\alpha-\gamma\right)\sin\left(\Delta m\left(t'+\delta t'\right)+\Delta\phi\right) + \Delta m\cos\left(\Delta m\left(t'+\delta t'\right)+\Delta\phi\right)\right]\right\} + \\
&\quad + \Delta m \left\{ e^{-\left(\bar{\Gamma}+\alpha-\gamma\right)t'} \left[\left(\bar{\Gamma}+\alpha-\gamma\right)\cos\left(\Delta m t'+\Delta\phi\right) - \Delta m \sin\left(\Delta m t'+\Delta\phi\right)\right] + \right. \\
&\quad \left.\left. + e^{-\left(\bar{\Gamma}+\alpha-\gamma\right)(t'+\delta t')} \left[-\left(\bar{\Gamma}+\alpha-\gamma\right)\cos\left(\Delta m\left(t'+\delta t'\right)+\Delta\phi\right) + \Delta m \sin\left(\Delta m\left(t'+\delta t'\right)+\Delta\phi\right)\right]\right\}\right\} + \\
&\quad + \frac{8\beta\left(e^{-\Gamma_S t'} - e^{-\Gamma_S(t'+\delta t')}\right)}{|d|\,|\bar{\eta}_{+-}| \left[\left(\bar{\Gamma}+\alpha-\gamma+\Gamma_S\right)^2 + (\Delta m)^2\right]\Gamma_S} \left[\left(\bar{\Gamma}+\alpha-\gamma+\Gamma_S\right)\sin(\Delta\phi) + \Delta m\cos(\Delta\phi)\right] +
\end{aligned}$$

$$-\frac{2}{\Gamma_S^2}\left(\frac{\gamma}{\Delta\Gamma\,|\bar{\eta}_{+-}|^2}+\frac{2\beta}{|d|\,|\bar{\eta}_{+-}|}\frac{\sin\phi_{+-}}{\cos\phi_{SW}}\right)\left(e^{-\Gamma_S t'}-e^{-\Gamma_S(t'+\delta t')}\right)\Bigg\}. \tag{46}$$

6.2.2 Smearing, efficiency, binning, range

Smearing matrix (Fig. 15) defines how the probabilities of reconstructing certain Δt values depend on actual Δt values. Efficiency histogram (Fig. 16) describes the probability of successful reconstruction, in this case for the $(\pi^+\pi^-, \pi^+\pi^-)$ decay channel, as a function of Δt. Both smearing matrix and values of efficiencies used in this work are the same as those used in KLOE analyses (obtained from Monte Carlo simulations). As indicated by Figures 15 and 16, the data were grouped in $1\tau_S$ bins, comparable with KLOE resolution [35].

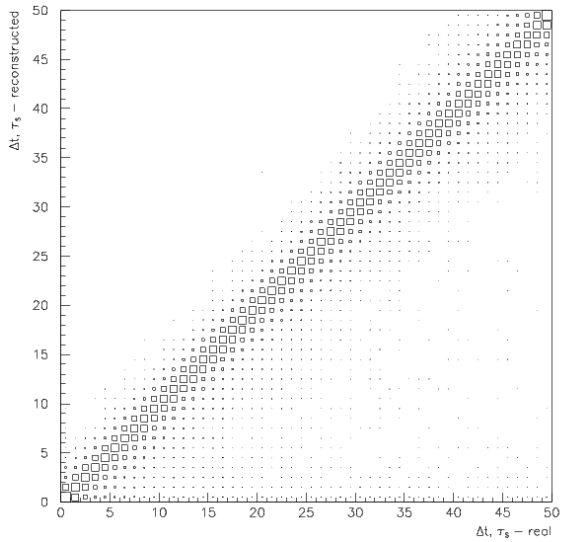

Figure 15: Smearing matrix presenting Δt reconstructed (vertical axis) vs. real (simulated, horizontal axis) values.

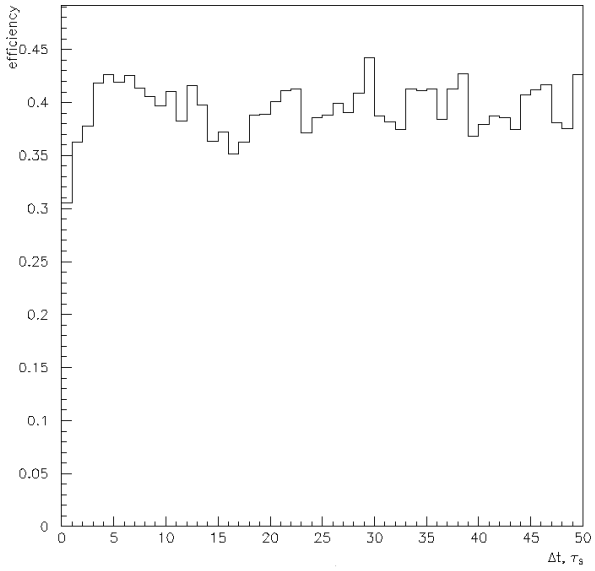

Figure 16: Efficiency for successful identification of $(\pi^+\pi^-, \pi^+\pi^-)$ decay as a function of time difference between the decays.

What differs significantly from KLOE analyses is the range in which the fits have been performed. In this work only time differences between 0 and $12\tau_S$ have been taken into account. This limit is justified by the observation, that for higher Δt values the decay rate shape is considerably influenced by K_S regeneration on the beam pipe. In KLOE analyses this effect was accounted for, which allowed fitting in the whole range covered by the smearing matrix, 0-$50\tau_S$.

6.2.3 Dealing with small numbers

In this section information about programming approach is presented. It is crucial for understanding the code in appendix B, however a reader uninterested in computational details can without much loss skip to section 6.3.

As α, β and γ parameters can be as small as 10^{-20} GeV, a special way of handling them in programs is needed so that they do not cause numerical problems. For this reason the following substitution were used in the code (the actual values are on the left side, the values used are after arrows):

$$\hbar = 6.58211915 \cdot 10^{-25}\ \text{GeV}\cdot\ \text{s} \longrightarrow \hbar = 6.58211915$$
$$\tau_S = 0.8958 \cdot 10^{-10}\ \text{s} \longrightarrow \tau_S = 0.8958$$
$$\tau_L = 511.6 \cdot 10^{-10}\ \text{s} \longrightarrow \tau_L = 511.6$$
$$\Delta m = 0.5920 \cdot 10^{10} \frac{\hbar}{\text{s}} \longrightarrow \Delta m = 0.529 \cdot \hbar$$

Using the above we can also write $\Gamma_S = \frac{\hbar}{\tau_S}$, $\Gamma_L = \frac{\hbar}{\tau_L}$ and introduce a time conversion constant $t_{cc} = \frac{\tau_S}{\hbar}$. After these redefinitions Γ_S, Γ_L and Δm are in the units of 10^{-15} GeV, while a product $t[\text{in } \tau_S \text{ units}]\cdot t_{cc}$ is in the units of 10^{15} GeV^{-1}.

6.2.4 Actual fitting function, normalisation

We start from modifying eq. (43) by multiplying every term with time by t_{cc}. Instead of (46) we get:

$$\begin{aligned}
&I_{t'}(\alpha,\beta,\gamma) = \\
&= |A_0|^4 |\bar{\eta}_{+-}|^2 \left\{ \frac{R_L}{|\bar{\eta}_{+-}|^2 \bar{\Gamma}} \left[\frac{1}{\Gamma_S t_{cc}} \left(e^{-\Gamma_S t_{cc} t'} - e^{-\Gamma_S t_{cc}(t'+\delta t')} \right) + \frac{1}{\Gamma_L t_{cc}} \left(e^{-\Gamma_L t_{cc} t'} - e^{-\Gamma_L t_{cc}(t'+\delta t')} \right) \right] + \right. \\
&- \frac{2}{\left(\bar{\Gamma}+\alpha-\gamma\right)\left[\left(\bar{\Gamma}+\alpha-\gamma\right)^2 + (\Delta m)^2\right] \cdot t_{cc}^2} \cdot \\
&\cdot \left[e^{-\left(\bar{\Gamma}+\alpha-\gamma\right) t_{cc}(t'+\delta t')} \left(\Delta m t_{cc} \sin\left(\Delta m t_{cc}\left(t'+\delta t'\right)\right) - \left(\bar{\Gamma}+\alpha-\gamma\right) t_{cc} \cos\left(\Delta m t_{cc}\left(t'+\delta t'\right)\right) \right) + \right. \\
&\left. - e^{-\left(\bar{\Gamma}+\alpha-\gamma\right) t_{cc} t'} \left(\Delta m t_{cc} \sin\left(\Delta m t_{cc} t'\right) - \left(\bar{\Gamma}+\alpha-\gamma\right) t_{cc} \cos\left(\Delta m t_{cc} t'\right) \right) \right] + \\
&+ \frac{8\beta}{|d|\,|\bar{\eta}_{+-}| \left[\left(\bar{\Gamma}+\alpha-\gamma+\Gamma_S\right)^2 + (\Delta m)^2\right] \left[\left(\bar{\Gamma}+\alpha-\gamma\right)^2 + (\Delta m)^2\right] \cdot t_{cc}^2} \cdot \\
&\cdot \left\{ \left(\bar{\Gamma}+\alpha-\gamma+\Gamma_S\right) \left\{ e^{-\left(\bar{\Gamma}+\alpha-\gamma\right) t_{cc} t'} \left[\left(\bar{\Gamma}+\alpha-\gamma\right) t_{cc} \sin\left(\Delta m t_{cc} t' + \Delta\phi\right) + \Delta m t_{cc} \cos\left(\Delta m t_{cc} t' + \Delta\phi\right) \right] + \right. \right. \\
&\left. - e^{-\left(\bar{\Gamma}+\alpha-\gamma\right) t_{cc}(t'+\delta t')} \left[\left(\bar{\Gamma}+\alpha-\gamma\right) t_{cc} \sin\left(\Delta m t_{cc}\left(t'+\delta t'\right) + \Delta\phi\right) + \Delta m t_{cc} \cos\left(\Delta m t_{cc}\left(t'+\delta t'\right) + \Delta\phi\right) \right] \right\} + \\
&+ \Delta m \left\{ e^{-\left(\bar{\Gamma}+\alpha-\gamma\right) t_{cc} t'} \left[\left(\bar{\Gamma}+\alpha-\gamma\right) t_{cc} \cos\left(\Delta m t_{cc} t' + \Delta\phi\right) - \Delta m t_{cc} \sin\left(\Delta m t_{cc} t' + \Delta\phi\right) \right] + \right. \\
&\left. \left. + e^{-\left(\bar{\Gamma}+\alpha-\gamma\right) t_{cc}(t'+\delta t')} \left[- \left(\bar{\Gamma}+\alpha-\gamma\right) t_{cc} \cos\left(\Delta m t_{cc}\left(t'+\delta t'\right) + \Delta\phi\right) + \Delta m t_{cc} \sin\left(\Delta m t_{cc}\left(t'+\delta t'\right) + \Delta\phi\right) \right] \right\} \right\} + \\
&+ \frac{8\beta \left(e^{-\Gamma_S t_{cc} t'} - e^{-\Gamma_S t_{cc}(t'+\delta t')} \right)}{|d|\,|\bar{\eta}_{+-}| \left[\left(\bar{\Gamma}+\alpha-\gamma+\Gamma_S\right)^2 + (\Delta m)^2\right] \Gamma_S t_{cc}} \left[\left(\bar{\Gamma}+\alpha-\gamma+\Gamma_S\right) \sin(\Delta\phi) + \Delta m \cos(\Delta\phi) \right] +
\end{aligned}$$

$$-\frac{2}{\Gamma_S^2 t_{cc}}\left(\frac{\gamma}{\Delta\Gamma\,|\bar{\eta}_{+-}|^2}+\frac{2\beta}{|d|\,|\bar{\eta}_{+-}|}\frac{\sin\phi_{+-}}{\cos\phi_{SW}}\right)\left(e^{-\Gamma_S t_{cc} t'}-e^{-\Gamma_S t_{cc}(t'+\delta t')}\right)\Bigg\}. \qquad (46')$$

The function (43) should be normalised before fitting in order to avoid any systematical effects from nonzero values of α, β and γ parameters. Here eq. (46') turns out to be really useful, as it is enough to substitute t' by zero and $t'+\delta t'$ by $\Delta t_{\max}$ (which in this case is $12\tau_S$). One then obtains a number by which function (43) should be divided to be normalised to unity.

6.3 Results, comparison with previously published (KLOE, CPLEAR)

6.3.1 Influence of the parameters upon the decay rate shape

To check how a nonzero value of each parameter separately would affect the decay rate curve the Figures 17, 18 and 19 were prepared. To exaggerate the result, the numbers taken for values of the parameters are approximately an order of magnitude bigger than the ones obtained in the CPLEAR experiment [49]. From these plots one can conclude that the curve is the least sensitive to α, that all three parameters can manifest themselves in the interference region, and that the plateau is mostly affected by β.

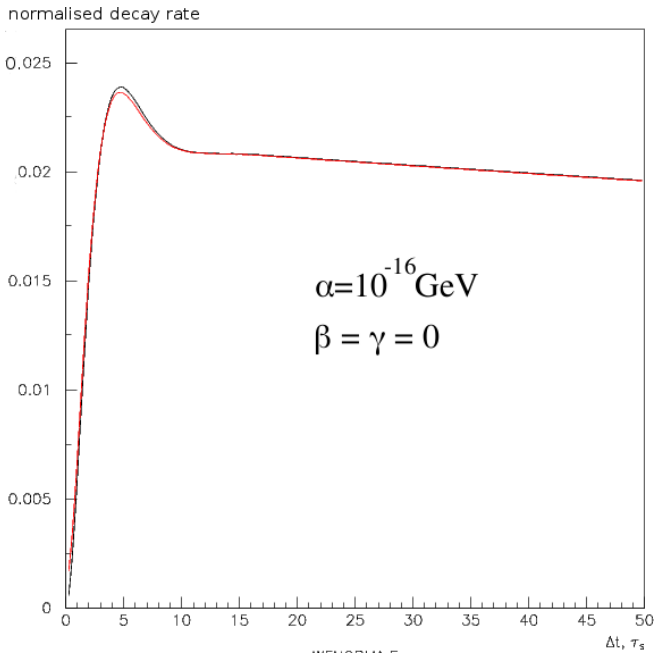

Figure 17: The effect of nonzero α value on the double decay rate shape. The black curve is for $\alpha=\beta=\gamma=0$ and the red for $\alpha=10^{-16}$ GeV, $\beta=\gamma=0$.

6.3.2 Fits with α, β and γ parameters

Three kinds of fits were performed. First, each of the three parameters was allowed to differ from zero with the other two parameters vanishing. Then a fit was made assuming complete positivity hypothesis ($\alpha=\gamma$, $\beta=0$). Finally a fit with all three parameters being free was performed. Each time normalisation was left as an extra parameter. The results are summarised in Tab. 4.

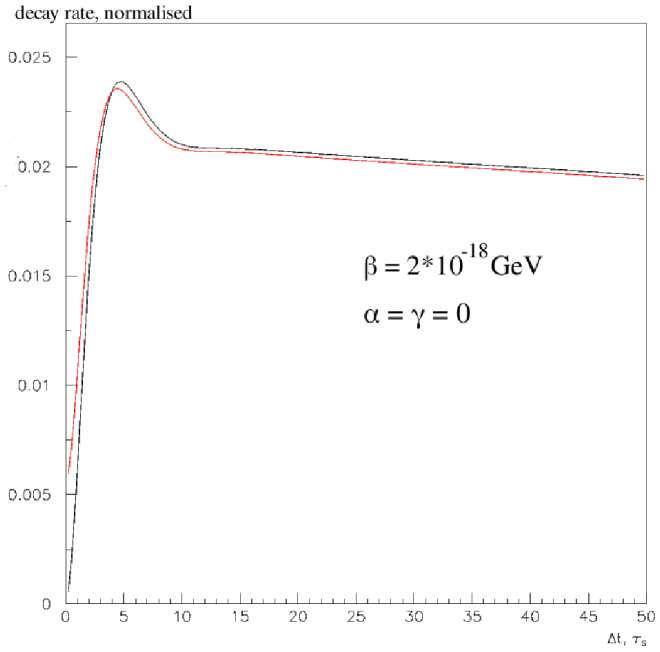

Figure 18: The effect of nonzero β value on the double decay rate shape. The black curve is for $\alpha = \beta = \gamma = 0$ and the red for $\beta = 2 \cdot 10^{-18}$ GeV, $\alpha = \gamma = 0$.

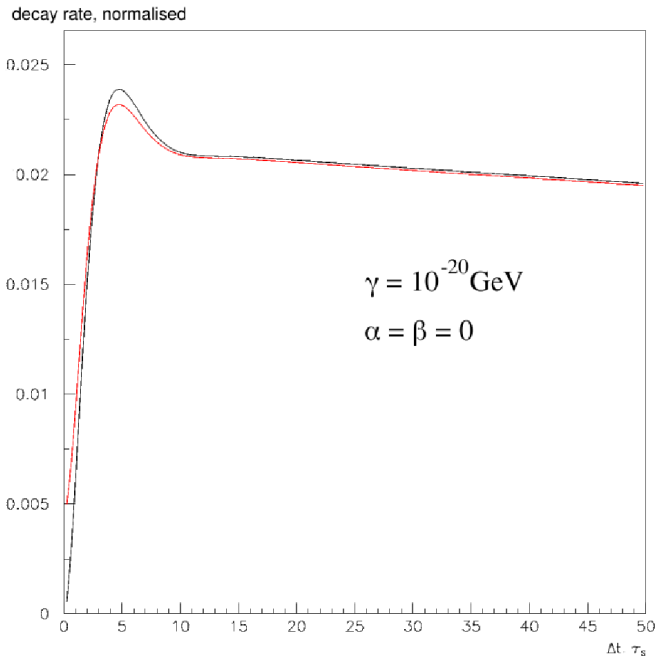

Figure 19: The effect of nonzero γ value on the double decay rate shape. The black curve is for $\alpha = \beta = \gamma = 0$ and the red for $\gamma = 10^{-20}$ GeV, $\alpha = \beta = 0$.

Table 4: Fit summary table.

Assumption	α, GeV	β, GeV	γ, GeV	χ^2/ndf	Figure
$\beta = \gamma = 0$	$(1.184 \pm 0.0013) \cdot 10^{-15}$	–	–	4.30	20
$\alpha = \gamma = 0$	–	$(1.26 \pm 0.11) \cdot 10^{-18}$	–	3.82	21
$\alpha = \beta = 0$	–	–	$(1.93 \pm 0.21) \cdot 10^{-20}$	2.02	22
$\alpha = \gamma$, $\beta = 0$	–	–	$(1.93 \pm 0.21) \cdot 10^{-20}$	2.02	23
–	$(2.662 \pm 0.0025) \cdot 10^{-16}$	$(-2.76 \pm 0.19) \cdot 10^{-18}$	$(4.25 \pm 0.21) \cdot 10^{-20}$	1.87	24

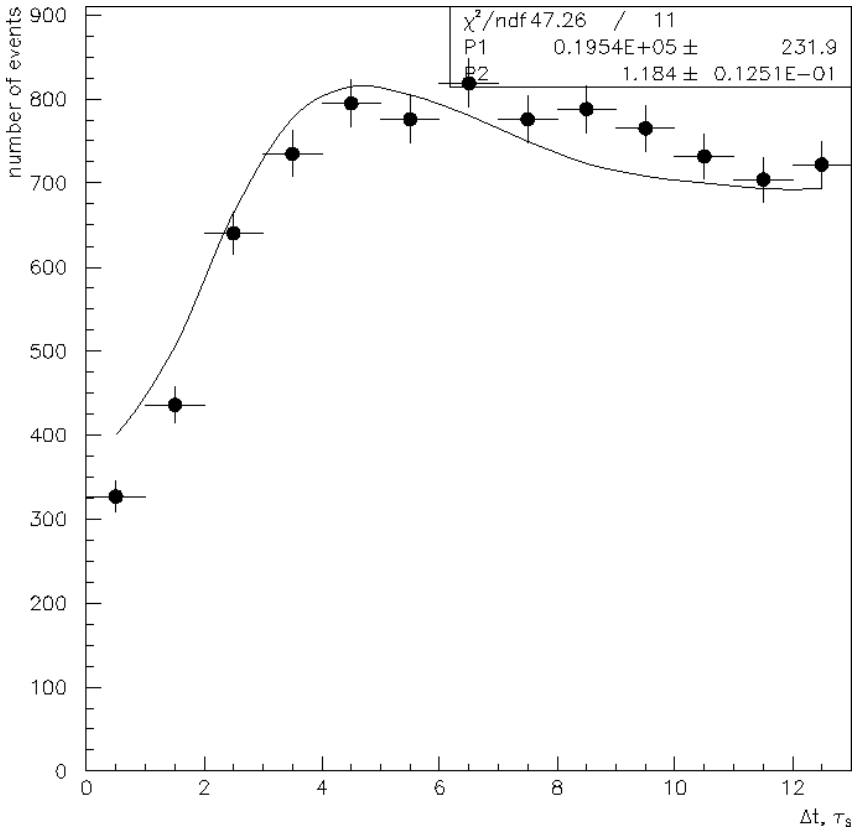

Figure 20: Fit with condition $\beta = \gamma = 0$.

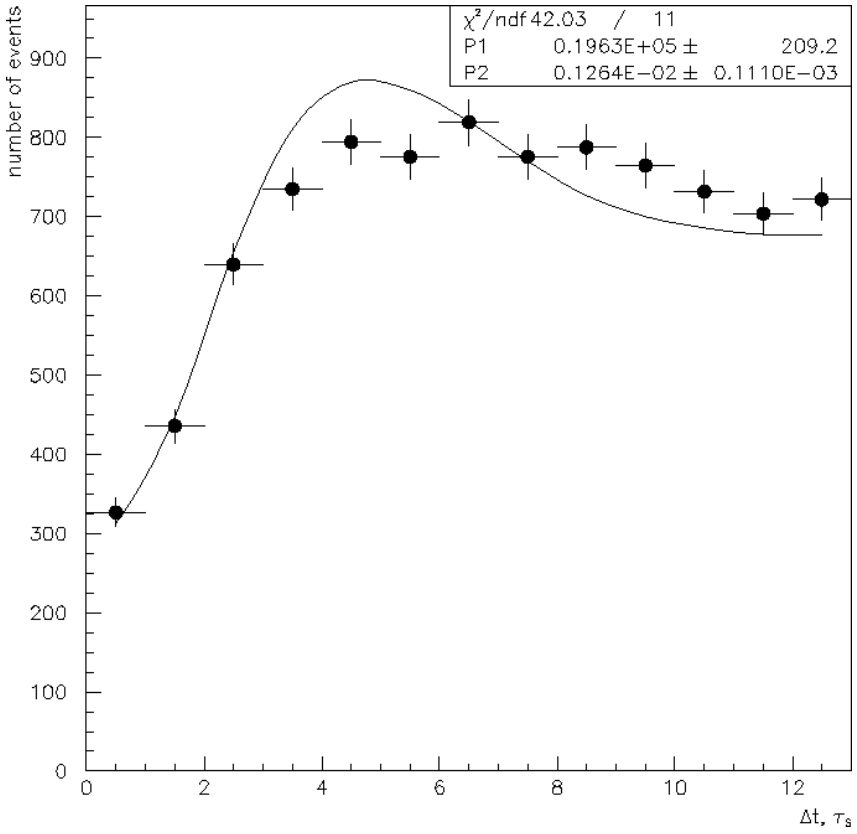

Figure 21: Fit with condition $\alpha = \gamma = 0$.

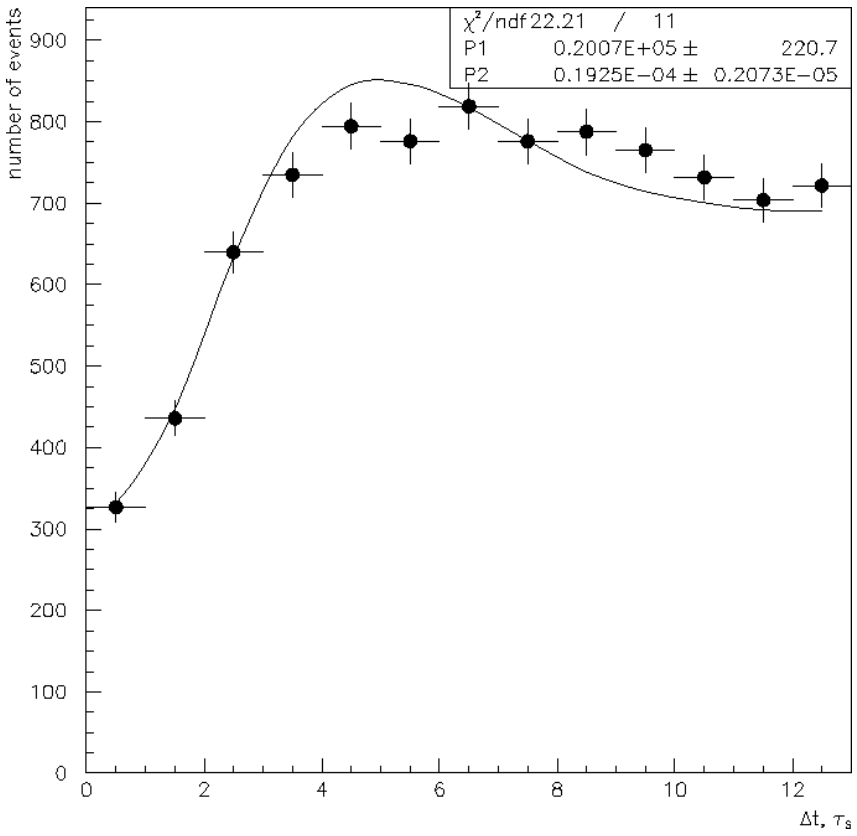

Figure 22: Fit with condition $\alpha = \beta = 0$.

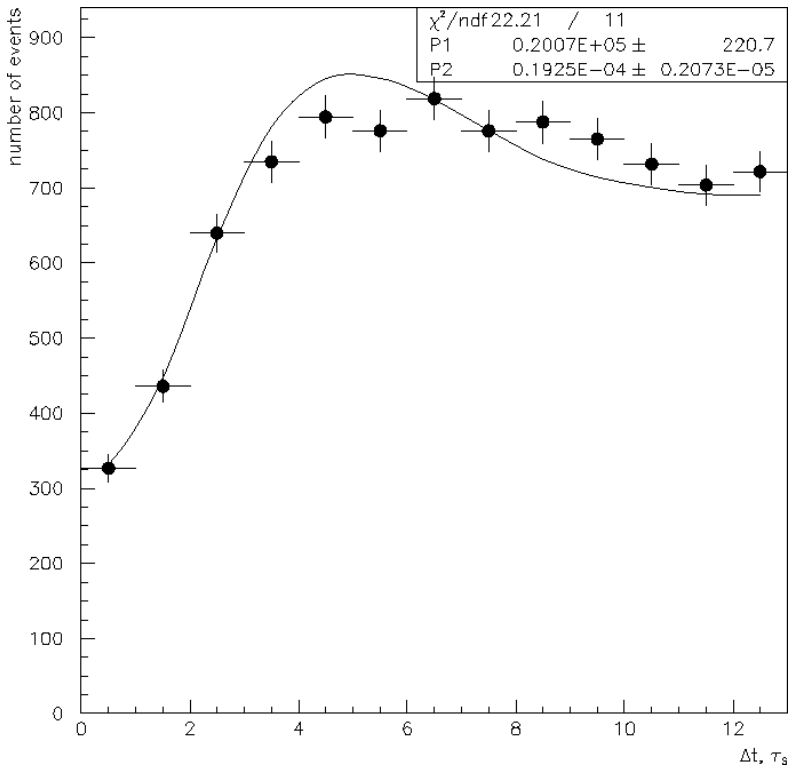

Figure 23: Fit with conditions $\alpha = \gamma$, $\beta = 0$.

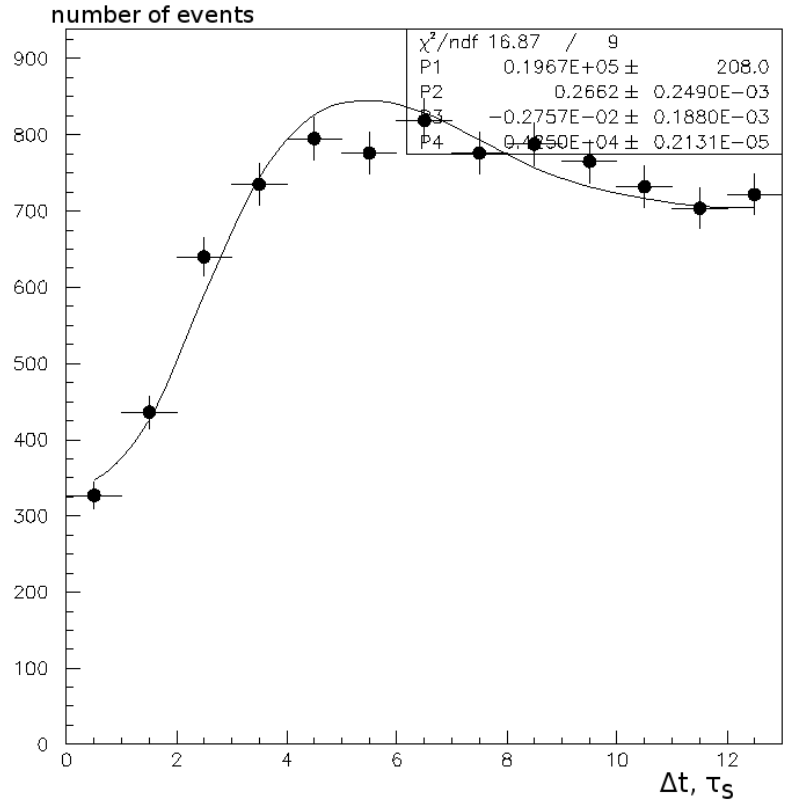

Figure 24: Fit of the function (43) to data.

The obtained values of paraeters can be compared with KLOE and CPLEAR results:

Table 5: Comparison with previous results for the fit with all parameters free.

	CPLEAR [49]	KLOE 2007 (2002 data) [7]	This work
α	$(-0.5 \pm 2.8) \cdot 10^{-17}$ GeV	$(-10^{+41}_{-31} \pm 9) \cdot 10^{-17}$ GeV	$(2.662 \pm 0.0025) \cdot 10^{-16}$ GeV
β	$(2.5 \pm 2.3) \cdot 10^{-19}$ GeV	$(3.7^{+6.9}_{-9.2} \pm 1.8) \cdot 10^{-19}$ GeV	$(-2.76 \pm 0.19) \cdot 10^{-18}$ GeV
γ	$(1.1 \pm 2.5) \cdot 10^{-21}$ GeV	$(-0.5^{+5.8}_{-5.1} \pm 1.2) \cdot 10^{-21}$ GeV	$(4.25 \pm 0.21) \cdot 10^{-20}$ GeV

Table 6: Comparison to previous results with $\alpha = \gamma$, $\beta = 0$ assumption.

KLOE [28]	This work
$\gamma = (0.7 \pm 1.2_{\mathrm{stat}} \pm 0.3_{\mathrm{syst}}) \cdot 10^{-21}$ GeV	$\gamma = (4.25 \pm 0.21) \cdot 10^{-20}$ GeV

One can notice that values obtained in this analysis are generally higher than than those obtained before, in some cases the difference is of one order of magnitude. However, these results should be treated as less significant than those from Ref. [49, 7, 28] for several reasons. Most importantly, the fit was performed only for the 0-12τ_S range, while in the KLOE analysis the range was 0-50τ_S, which was made possible by accounting for K_S regeneration on the beam pipe. What also matters is that here only a subset of all gathered data was used, namely the data from the year 2005. A small difference in favour of this analysis is that for the KLOE fit the integral (46) was only estimated, not obtained analytically.

While KLOE and CPLEAR experiments gave only the upper bounds for the α, β and γ values, there are also predictions for their lower limits. For instance, a prediction that will probably be verified by the KLOE-2 experiment is given in Ref. [50]. Assuming that the so-called "solar neutrino problem" (deficit of observed neutrinos from the Sun with respect to the theoretically expected amount) is only due to mechanism of evolution from pure into mixed states, the authors derived:

$$\begin{aligned} \gamma &\geq 7.4 \cdot 10^{-22} \text{ GeV} \qquad \text{for } \alpha < 2\gamma, \\ \alpha &\geq 1.5 \cdot 10^{-21} \text{ GeV} \qquad \text{for } \alpha > 2\gamma. \end{aligned} \tag{47}$$

7 Summary

One of the goals of this thesis was to describe the time evolution of quantum entangled kaon pairs in a way intelligible for a reader unfamiliar with the physics of kaons. For this reason many calculations and examples of Fortran code used in programs have been included in the appendix.

CPT symmetry has not been observed to be violated. Nevertheless, several parameterisations have been invented that allow for its noninvariance for different reasons. One of the ideas is that CPT might be violated by the evolution from pure to mixed states induced by quantum gravity effects. This is especially interesting, as although the concept has been known for a long time, a theory of quantum gravity still eludes us and when describing it we have to rely on intuition rather than on solid theoretical ground.

An approach was made to analyse a subset of KLOE data for the effects of quantum gravity. The results obtained, although less significant than KLOE and CPLEAR ones, encourage further measurements, as they indicate that precision expected in KLOE-2 experiment may be high enough to verify at least a fraction of theoretical predictions.

Kaons seem to have a patent for breaking symmetries. With more and more precise tests, we may soon for the first time witness a violation of the CPT symmetry thanks to the KLOE-2 data. Even if not, this experiment is certain to deepen our understanding of these fascinating particles.

A Calculations

A.1 Calculations for chapter 2

A.1.1 Eigenvalues

Hamiltonian from eq. (5) can be written using explicitly real and imaginary parts of $\mathbf{M}$ and $\mathbf{\Gamma}$ matrices:

$$\mathbf{H} = \begin{pmatrix} \Re M_{11} + \frac{1}{2}\Im\Gamma_{11} + i\left(\Im M_{11} - \frac{1}{2}\Re\Gamma_{11}\right) & \Re M_{12} + \frac{1}{2}\Im\Gamma_{12} + i\left(\Im M_{12} - \frac{1}{2}\Re\Gamma_{12}\right) \\ \Re M_{12} - \frac{1}{2}\Im\Gamma_{12} - i\left(\Im M_{12} + \frac{1}{2}\Re\Gamma_{12}\right) & \Re M_{22} + \frac{1}{2}\Im\Gamma_{22} + i\left(\Im M_{22} - \frac{1}{2}\Re\Gamma_{22}\right) \end{pmatrix}$$

We now move to equation for Δ (11). In the CPT limit (6) $H_{11} = H_{22}$, so Δ is reduced to:

$$\Delta = 4H_{12}H_{21}.$$

We further simplify this expression by going to CP limit, which means we assume that the phases of M_{12} and Γ_{12} are the same. We can then write:

$$M_{12} = |M_{12}|\cos\phi + i\,|M_{12}|\sin\phi, \qquad \Gamma_{12} = |\Gamma_{12}|\cos\phi + i\,|\Gamma_{12}|\sin\phi.$$

Using the above we rewrite H_{12} and H_{21}:

$$H_{12} = |M_{12}|\cos\phi + \frac{1}{2}|\Gamma_{12}|\sin\phi + i\left(|M_{12}|\sin\phi - \frac{1}{2}|\Gamma_{12}|\cos\phi\right)$$
$$H_{21} = |M_{12}|\cos\phi - \frac{1}{2}|\Gamma_{12}|\sin\phi - i\left(|M_{12}|\sin\phi + \frac{1}{2}|\Gamma_{12}|\cos\phi\right),$$

so the product $H_{12}H_{21}$ equals:

$$\begin{aligned} H_{12}H_{21} = {} & |M_{12}|^2\cos^2\phi - \frac{1}{2}|M_{12}\Gamma_{12}|\sin\phi\cos\phi - i\,|M_{12}|^2\sin\phi\cos\phi - \frac{i}{2}|M_{12}\Gamma_{12}|\cos^2\phi + \\ & + \frac{1}{2}|M_{12}\Gamma_{12}|\sin\phi\cos\phi - \frac{1}{4}|\Gamma_{12}|^2\sin^2\phi - \frac{i}{2}|M_{12}\Gamma_{12}|\sin^2\phi - \frac{i}{4}|\Gamma_{12}|^2\sin\phi\cos\phi + \\ & + i\,|M_{12}|^2\sin\phi\cos\phi - \frac{i}{2}|M_{12}\Gamma_{12}|\sin^2\phi + |M_{12}|^2\sin^2\phi + \frac{1}{2}|M_{12}\Gamma_{12}|\sin\phi\cos\phi + \\ & - \frac{i}{2}|M_{12}\Gamma_{12}|\cos^2\phi + \frac{i}{4}|\Gamma_{12}|^2\sin\phi\cos\phi - \frac{1}{2}|M_{12}\Gamma_{12}|\sin\phi\cos\phi - \frac{1}{4}|\Gamma_{12}|^2\cos^2\phi \end{aligned}$$

It is easy to check that the terms with $\sin\phi\cos\phi$ cancel out, and what remains gives:

$$\begin{aligned} H_{12}H_{21} &= |M_{12}|^2 - \frac{1}{4}|\Gamma_{12}|^2 - i\,|M_{12}\Gamma_{12}| = \\ &= \left(|M_{12}|^2 + \frac{1}{4}|\Gamma_{12}|^2\right)\exp\left[-i\arcsin\left(\frac{|M_{12}\Gamma_{12}|}{|M_{12}|^2 + \frac{1}{4}|\Gamma_{12}|^2}\right)\right]. \end{aligned}$$

Now we can return to the discriminant Δ:

$$\Delta = 4\left(|M_{12}|^2 + \frac{1}{4}|\Gamma_{12}|^2\right)\exp\left[-i\arcsin\left(\frac{|M_{12}\Gamma_{12}|}{|M_{12}|^2 + \frac{1}{4}|\Gamma_{12}|^2}\right)\right],$$

$$\sqrt{\Delta} = 2\sqrt{|M_{12}|^2 + \frac{1}{4}|\Gamma_{12}|^2}\exp\left[-\frac{i}{2}\arcsin\left(\frac{|M_{12}\Gamma_{12}|}{|M_{12}|^2 + \frac{1}{4}|\Gamma_{12}|^2}\right)\right],$$

and the eigenvalues are of the form of the usual quadratic equation solutions:

$$\lambda_\pm = \frac{H_{11} + H_{22} \pm \sqrt{\Delta}}{2}$$

A.1.2 Eigenstates

The equation for eigenvectors is of the standard form:

$$\begin{pmatrix} H_{11}-\lambda_\pm & H_{12} \end{pmatrix} \begin{pmatrix} u_\pm \\ w_\pm \end{pmatrix} = 0.$$

From this we find the relation between $u_\pm$ and $w_\pm$:

$$(H_{11}-\lambda_\pm)\,u_\pm + H_{12}w_\pm = 0 \quad \Longrightarrow \quad \frac{w_\pm}{u_\pm} = \frac{\lambda_\pm - H_{11}}{H_{12}} \overset{CPT}{=\!=} \pm\sqrt{\frac{H_{21}}{H_{12}}}$$

In the symmetric limit of exact CP ($\arg\frac{\Gamma_{12}}{M_{12}}=0$) we have [11]:

$$\frac{H_{12}}{H_{21}} = \frac{M_{12}-\frac{i}{2}\Gamma_{12}}{M_{12}^*-\frac{i}{2}\Gamma_{12}^*} = \frac{M_{12}}{M_{12}^*} = \text{ phase factor } \overset{\text{def}}{=\!=} e^{-2i\alpha}.$$

Using the above, the eigenvectors are found to be:

- for λ_+ we have $w_+ = e^{i\alpha}u_+$, so:

$$v_+ := \begin{pmatrix} u_+ \\ w_+ \end{pmatrix} = u_+ \begin{pmatrix} 1 \\ e^{i\alpha} \end{pmatrix} = u_+ e^{i\frac{\alpha}{2}} \begin{pmatrix} e^{-i\frac{\alpha}{2}} \\ e^{i\frac{\alpha}{2}} \end{pmatrix}$$

- for λ_- we have $u_- = -w_- e^{-i\alpha}$, so:

$$v_- := \begin{pmatrix} u_- \\ w_- \end{pmatrix} = -w_- \begin{pmatrix} e^{-i\alpha} \\ -1 \end{pmatrix} = -w_- e^{-i\frac{\alpha}{2}} \begin{pmatrix} e^{-i\frac{\alpha}{2}} \\ -e^{i\frac{\alpha}{2}} \end{pmatrix}$$

A.2 Calculations for chapter 3

A.2.1 $|i\rangle$ as a function of $|K_S\rangle, |K_L\rangle$

Calculations presented here are rather basic, but they are given for completeness.

For the sake of brevity let us denote: $\alpha^{-1} := \sqrt{2\left(1+|\epsilon_S|^2\right)}$, $\beta^{-1} := \sqrt{2\left(1+|\epsilon_L|^2\right)}$ and $\gamma := 1-\epsilon_S\epsilon_L$. Using these variables we can rewrite (18):

$$\begin{aligned} |K_S\rangle &= \alpha\left[(1+\epsilon_S)\left|K^0\right\rangle + (1-\epsilon_S)\left|\bar{K}^0\right\rangle\right], \\ |K_L\rangle &= \beta\left[(1+\epsilon_L)\left|K^0\right\rangle - (1-\epsilon_L)\left|\bar{K}^0\right\rangle\right] \end{aligned}$$

From this we obtain $\left|K^0\right\rangle$ and $\left|\bar{K}^0\right\rangle$ expressed by $|K_S\rangle$ and $|K_L\rangle$:

$$\begin{aligned} \left|K^0\right\rangle &= \frac{1-\epsilon_L}{2\alpha\gamma}|K_S\rangle + \frac{1-\epsilon_S}{2\beta\gamma}|K_L\rangle, \\ \left|\bar{K}^0\right\rangle &= \frac{1+\epsilon_L}{2\alpha\gamma}|K_S\rangle - \frac{1+\epsilon_S}{2\beta\gamma}|K_L\rangle, \end{aligned}$$

so the initial state is:

$$\begin{aligned} |i\rangle = \frac{1}{\sqrt{2}}\Bigg(&\left[\frac{1-\epsilon_L}{2\alpha\gamma}|K_S(-\vec{p})\rangle + \frac{1-\epsilon_S}{2\beta\gamma}|K_L(-\vec{p})\rangle\right]\cdot\left[\frac{1+\epsilon_L}{2\alpha\gamma}|K_S(+\vec{p})\rangle - \frac{1+\epsilon_S}{2\beta\gamma}|K_L(+\vec{p})\rangle\right] + \\ &- \left[\frac{1+\epsilon_L}{2\alpha\gamma}|K_S(-\vec{p})\rangle - \frac{1+\epsilon_S}{2\beta\gamma}|K_L(-\vec{p})\rangle\right]\cdot\left[\frac{1-\epsilon_L}{2\alpha\gamma}|K_S(+\vec{p})\rangle + \frac{1-\epsilon_S}{2\beta\gamma}|K_L(+\vec{p})\rangle\right]\Bigg). \end{aligned}$$

It is easy to see that the terms with products $|K_S(+\vec{p})\rangle |K_S(-\vec{p})\rangle$ and $|K_L(+\vec{p})\rangle |K_L(-\vec{p})\rangle$ cancel out, so the above equation gives:

$$\begin{aligned}|i\rangle &= \frac{1}{4\sqrt{2}\alpha\beta\gamma^2}\{[(1+\epsilon_L)(1-\epsilon_S)+(1-\epsilon_L)(1+\epsilon_S)]\,|K_S(+\vec{p})\rangle\,|K_L(-\vec{p})\rangle + \\ &\quad -[(1+\epsilon_S)(1-\epsilon_L)+(1-\epsilon_S)(1+\epsilon_L)]\,|K_L(+\vec{p})\rangle\,|K_S(-\vec{p})\rangle\} = \\ &= \frac{1}{4\sqrt{2}\alpha\beta\gamma^2}\{2\gamma\,|K_S(+\vec{p})\rangle\,|K_L(-\vec{p})\rangle - 2\gamma\,|K_L(+\vec{p})\rangle\,|K_S(-\vec{p})\rangle\} = \\ &= \frac{1}{2\sqrt{2}\alpha\beta\gamma}\{|K_S(+\vec{p})\rangle\,|K_L(-\vec{p})\rangle - |K_L(+\vec{p})\rangle\,|K_S(-\vec{p})\rangle\}\end{aligned}$$

Therefore we can write:

$$|i\rangle = \frac{N}{\sqrt{2}}\{|K_S(+\vec{p})\rangle\,|K_L(-\vec{p})\rangle - |K_L(+\vec{p})\rangle\,|K_S(-\vec{p})\rangle\}$$

where N, $N=(2\alpha\beta\gamma)^{-1}$, written in original variables ϵ_S, ϵ_L is:

$$N = \frac{\sqrt{2\left(1+|\epsilon_S|^2\right)}\sqrt{2\left(1+|\epsilon_L|^2\right)}}{2(1-\epsilon_S\epsilon_L)} = \frac{\sqrt{\left(1+|\epsilon_S|^2\right)\left(1+|\epsilon_L|^2\right)}}{1-\epsilon_S\epsilon_L} \approx 1.$$

A.2.2 Double decay rate $I(f_1,t_1;f_2,t_2)$

We want to obtain eq. (26). We have:

$$\begin{aligned}&I(f_1,t_1;f_2,t_2) = A(f_1,t_1;f_2,t_2)\,A^*(f_1,t_1;f_2,t_2) = \\ &= \frac{|N|^2}{2}\Big\{\langle f_1|T|K_S\rangle\langle f_2|T|K_L\rangle\langle f_1|T|K_S\rangle^*\langle f_2|T|K_L\rangle^* e^{-\Gamma_S t_1-\Gamma_L t_2} + \\ &+\langle f_1|T|K_L\rangle\langle f_2|T|K_S\rangle\langle f_1|T|K_L\rangle^*\langle f_2|T|K_S\rangle^* e^{-\Gamma_L t_1-\Gamma_S t_2} + \\ &-\langle f_1|T|K_S\rangle\langle f_2|T|K_L\rangle\langle f_1|T|K_L\rangle^*\langle f_2|T|K_S\rangle^* e^{i(m_L-m_S)t_1-i(m_L-m_S)t_2}e^{-\frac{\Gamma_S}{2}(t_1+t_2)-\frac{\Gamma_L}{2}(t_1+t_2)} + \\ &-\langle f_1|T|K_L\rangle\langle f_2|T|K_S\rangle\langle f_1|T|K_S\rangle^*\langle f_2|T|K_L\rangle^* e^{-i(m_L-m_S)t_1+i(m_L-m_S)t_2}e^{-\frac{\Gamma_S}{2}(t_1+t_2)-\frac{\Gamma_L}{2}(t_1+t_2)}\Big\} = \\ &= \frac{|N|^2}{2}\Big\{|\langle f_1|T|K_S\rangle\langle f_2|T|K_L\rangle|^2 e^{-\Gamma_S t_1-\Gamma_L t_2} + |\langle f_1|T|K_L\rangle\langle f_2|T|K_S\rangle|^2 e^{-\Gamma_L t_1-\Gamma_S t_2} + \\ &-\langle f_1|T|K_S\rangle\langle f_2|T|K_L\rangle\langle f_1|T|K_L\rangle^*\langle f_2|T|K_S\rangle^* e^{i\Delta m(t_1-t_2)}e^{-\frac{\Gamma_S+\Gamma_L}{2}(t_1+t_2)} + \\ &-\langle f_1|T|K_L\rangle\langle f_2|T|K_S\rangle\langle f_1|T|K_S\rangle^*\langle f_2|T|K_L\rangle^* e^{-i\Delta m(t_1-t_2)}e^{-\frac{\Gamma_S+\Gamma_L}{2}(t_1+t_2)}\Big\} = \\ &= \frac{|N|^2}{2}\left(\left|\langle f_1|T|K_S\rangle\langle f_2|T|K_S\rangle\frac{\langle f_2|T|K_L\rangle}{\langle f_2|T|K_S\rangle}\right|^2 e^{-\Gamma_S t_1-\Gamma_L t_2} + \right. \\ &+\left|\frac{\langle f_1|T|K_L\rangle}{\langle f_1|T|K_S\rangle}\langle f_1|T|K_S\rangle\langle f_2|T|K_S\rangle\right|^2 e^{-\Gamma_L t_1-\Gamma_S t_2} + \\ &-\langle f_1|T|K_S\rangle\langle f_1|T|K_S\rangle^*\frac{\langle f_1|T|K_L\rangle^*}{\langle f_1|T|K_S\rangle^*}\langle f_2|T|K_S\rangle^*\langle f_2|T|K_S\rangle\frac{\langle f_2|T|K_L\rangle}{\langle f_2|T|K_S\rangle}\cdot e^{i\Delta m(t_1-t_2)}e^{-\frac{\Gamma_S+\Gamma_L}{2}(t_1+t_2)} + \\ &\left.-\frac{\langle f_1|T|K_L\rangle}{\langle f_1|T|K_S\rangle}\langle f_1|T|K_S\rangle\langle f_1|T|K_S\rangle^*\langle f_2|T|K_S\rangle\langle f_2|T|K_S\rangle^*\frac{\langle f_2|T|K_L\rangle^*}{\langle f_2|T|K_S\rangle^*}\cdot e^{-i\Delta m(t_1-t_2)}e^{-\frac{\Gamma_S+\Gamma_L}{2}(t_1+t_2)}\right) = \\ &= \frac{|N|^2}{2}|\langle f_1|T|K_S\rangle\langle f_2|T|K_S\rangle|^2\cdot\left(\left|\frac{\langle f_2|T|K_L\rangle}{\langle f_2|T|K_S\rangle}\right|^2 e^{-\Gamma_S t_1-\Gamma_L t_2} + \left|\frac{\langle f_1|T|K_L\rangle}{\langle f_1|T|K_S\rangle}\right|^2 e^{-\Gamma_L t_1-\Gamma_S t_2} + \right. \\ &\left.-\left[\left(\frac{\langle f_1|T|K_L\rangle}{\langle f_1|T|K_S\rangle}\right)^*\frac{\langle f_2|T|K_L\rangle}{\langle f_2|T|K_S\rangle}e^{i\Delta m(t_1-t_2)} + \frac{\langle f_1|T|K_L\rangle}{\langle f_1|T|K_S\rangle}\left(\frac{\langle f_2|T|K_L\rangle}{\langle f_2|T|K_S\rangle}\right)^* e^{-i\Delta m(t_1-t_2)}\right]e^{-\frac{\Gamma_S+\Gamma_L}{2}(t_1+t_2)}\right)\end{aligned}$$

It is now convenient to define C_{12} and η_i, see eqs. (27) and (28). Using these quantities we can write:

$$\begin{aligned}
I(f_1,t_1;f_2,t_2) &= C_{12}\Big\{|\eta_1|^2 e^{-\Gamma_L t_1-\Gamma_S t_2}+|\eta_2|^2 e^{-\Gamma_S t_1-\Gamma_L t_2}+\\
&\quad -\Big[|\eta_1|e^{-i\phi_1}|\eta_2|e^{i\phi_2}e^{i\Delta m(t_1-t_2)}+|\eta_1|e^{i\phi_1}|\eta_2|e^{-i\phi_2}e^{-i\Delta m(t_1-t_2)}\Big]e^{-\frac{\Gamma_S+\Gamma_L}{2}(t_1-t_2)}\Big\}=\\
&= C_{12}\Big\{|\eta_1|^2 e^{-\Gamma_L t_1-\Gamma_S t_2}+|\eta_2|^2 e^{-\Gamma_S t_1-\Gamma_L t_2}+\\
&\quad -|\eta_1||\eta_2|\Big[e^{i[\Delta m(t_1-t_2)+\phi_2-\phi_1]}+e^{-i[\Delta m(t_1-t_2)+\phi_2-\phi_1]}\Big]e^{-\frac{\Gamma_S+\Gamma_L}{2}(t_1-t_2)}\Big\}=\\
&= C_{12}\Big\{|\eta_1|^2 e^{-\Gamma_L t_1-\Gamma_S t_2}+|\eta_2|^2 e^{-\Gamma_S t_1-\Gamma_L t_2}+\\
&\quad -2|\eta_1||\eta_2|e^{-\frac{\Gamma_S+\Gamma_L}{2}(t_1-t_2)}\cos\left[\Delta m(t_1-t_2)+\phi_2-\phi_1\right]\Big\},
\end{aligned}$$

where we have used the fact that $\cos\alpha=\frac{e^{i\alpha}+e^{-i\alpha}}{2}$.

A.2.3 Double decay rates $I(f_1,f_2,\Delta t)$

Our starting point is eq. (26). Substituting $t=t_1+t_2,\quad \Delta t=t_1-t_2;\qquad t_1=\frac{t+\Delta t}{2},\quad t_2=\frac{t-\Delta t}{2}$ we obtain:

$$\begin{aligned}
I(f_1,f_2,t,\Delta t) &= C_{12}\Big\{|\eta_1|^2 e^{-\Gamma_L\frac{t+\Delta t}{2}}e^{-\Gamma_S\frac{t-\Delta t}{2}}+|\eta_2|^2 e^{-\Gamma_S\frac{t+\Delta t}{2}}e^{-\Gamma_L\frac{t-\Delta t}{2}}+\\
&\quad -2|\eta_1||\eta_2|e^{-\frac{\Gamma_S+\Gamma_L}{2}t}\cos\left[\Delta m\Delta t+\phi_2-\phi_1\right]\Big\}=\\
&= C_{12}\Big\{|\eta_1|^2 e^{-\frac{\Gamma_L}{2}t}e^{-\frac{\Gamma_L}{2}\Delta t}e^{-\frac{\Gamma_S}{2}t}e^{\frac{\Gamma_S}{2}\Delta t}+|\eta_2|^2 e^{-\frac{\Gamma_S}{2}t}e^{-\frac{\Gamma_S}{2}\Delta t}e^{-\frac{\Gamma_L}{2}t}e^{\frac{\Gamma_L}{2}\Delta t}+\\
&\quad -2|\eta_1||\eta_2|e^{-\frac{\Gamma_S+\Gamma_L}{2}t}\cos\left[\Delta m\Delta t+\phi_2-\phi_1\right]\Big\}=\\
&= C_{12}\Big\{|\eta_1|^2 e^{-\frac{\Gamma_L+\Gamma_S}{2}t}e^{-\frac{\Gamma_L-\Gamma_S}{2}\Delta t}+|\eta_2|^2 e^{-\frac{\Gamma_S+\Gamma_L}{2}t}e^{\frac{\Gamma_L-\Gamma_S}{2}\Delta t}+\\
&\quad -2|\eta_1||\eta_2|e^{-\frac{\Gamma_S+\Gamma_L}{2}t}\cos\left[\Delta m\Delta t+\phi_2-\phi_1\right]\Big\}=\\
&= C_{12}\Big\{|\eta_1|^2 e^{-\frac{\Gamma_L-\Gamma_S}{2}\Delta t}+|\eta_2|^2 e^{\frac{\Gamma_L-\Gamma_S}{2}\Delta t}+\\
&\quad -2|\eta_1||\eta_2|\cos\left[\Delta m\Delta t+\phi_2-\phi_1\right]\Big\}e^{-\frac{\Gamma_L+\Gamma_S}{2}t}.
\end{aligned}$$

Since we want to get rid of the dependence on $t=t_1+t_2$, we integrate the last equation in this variable. We observe that for non-negative numbers t_1, t_2 such that $t_1\geq t_2$ we always have $t_1+t_2\geq t_1-t_2$ and similarly we have $t_1+t_2\geq|t_1-t_2|$ for $t_1\leq t_2$. So if we divide this integral into two parts, one of them satysfying the condition $\Delta t\geq 0$ and the other $\Delta t\leq 0$, the lower limits will be Δt and $|\Delta t|$ respectively and infinity will be the upper limit in both cases.

The Jacobian matrix for transformation from t_1, t_2 to t, Δt coordinates is:

$$jac(t_1,t_2\to\Delta t,T)=\left|\left|\begin{array}{cc}\frac{\partial t_1}{\partial T} & \frac{\partial t_1}{\partial\Delta t}\\ \frac{\partial t_2}{\partial T} & \frac{\partial t_2}{\partial\Delta t}\end{array}\right|\right|.$$

Knowing that $t_1=\frac{t+\Delta t}{2}$ and $t_2=\frac{t-\Delta t}{2}$ and performing simple calculations we get $jac(t_1,t_2\to\Delta t,t)=\frac{1}{2}$.

Taking that into account we can finally write:

- for $\Delta t \geq 0$:

$$
\begin{aligned}
I\left(f_1, f_2, \Delta t \geq 0\right) &= jac\left(t_1{,}t_2 \rightarrow \Delta t{,}t\right) \cdot \int\limits_{\Delta t}^{\infty} I\left(f_1, f_2, \Delta t, t\right) dt = \\
&= \frac{1}{2} \int\limits_{\Delta t}^{\infty} C_{12} \Big\{ \left|\eta_1\right|^2 e^{-\frac{\Gamma_L - \Gamma_S}{2} \Delta t} + \left|\eta_2\right|^2 e^{\frac{\Gamma_L - \Gamma_S}{2} \Delta t} + \\
&\quad - 2 \left|\eta_1\right| \left|\eta_2\right| \cos\left[\Delta m \Delta t + \phi_2 - \phi_1\right] \Big\} e^{-\frac{\Gamma_L + \Gamma_S}{2} t} dt = \\
&= \frac{1}{2} C_{12} \Big\{ \left|\eta_1\right|^2 e^{-\frac{\Gamma_L - \Gamma_S}{2} \Delta t} + \left|\eta_2\right|^2 e^{\frac{\Gamma_L - \Gamma_S}{2} \Delta t} + \\
&\quad - 2 \left|\eta_1\right| \left|\eta_2\right| \cos\left[\Delta m \Delta t + \phi_2 - \phi_1\right] \Big\} \int\limits_{\Delta t}^{\infty} e^{-\frac{\Gamma_L + \Gamma_S}{2} t} dt = \\
&= \frac{1}{2} C_{12} \Big\{ \left|\eta_1\right|^2 e^{-\frac{\Gamma_L - \Gamma_S}{2} \Delta t} + \left|\eta_2\right|^2 e^{\frac{\Gamma_L - \Gamma_S}{2} \Delta t} + \\
&\quad - 2 \left|\eta_1\right| \left|\eta_2\right| \cos\left[\Delta m \Delta t + \phi_2 - \phi_1\right] \Big\} \cdot \left[-\frac{2}{\Gamma_L + \Gamma_S} e^{-\frac{\Gamma_L + \Gamma_S}{2} t} \right]_{t=\Delta t}^{t=\infty} = \\
&= \frac{1}{2} C_{12} \Big\{ \left|\eta_1\right|^2 e^{-\frac{\Gamma_L - \Gamma_S}{2} \Delta t} + \left|\eta_2\right|^2 e^{\frac{\Gamma_L - \Gamma_S}{2} \Delta t} + \\
&\quad - 2 \left|\eta_1\right| \left|\eta_2\right| \cos\left[\Delta m \Delta t + \phi_2 - \phi_1\right] \Big\} \cdot \frac{2}{\Gamma_L + \Gamma_S} e^{-\frac{\Gamma_L + \Gamma_S}{2} \Delta t} = \\
&= \frac{C_{12}}{\Gamma_S + \Gamma_L} \Big\{ \left|\eta_1\right|^2 e^{-\Gamma_L \Delta t} + \left|\eta_2\right|^2 e^{-\Gamma_S \Delta t} + \\
&\quad - 2 \left|\eta_1\right| \left|\eta_2\right| e^{-\frac{\Gamma_S + \Gamma_L}{2} \Delta t} \cos\left[\Delta m \Delta t + \phi_2 - \phi_1\right] \Big\},
\end{aligned}
$$

- similarly for $\Delta t \leq 0$:

$$
\begin{aligned}
I\left(f_1, f_2, \Delta t \leq 0\right) &= jac\left(t_1{,}t_2 \rightarrow \Delta t{,}t\right) \cdot \int\limits_{|\Delta t|}^{\infty} I\left(f_1, f_2, \Delta t, t\right) dt = \\
&= \frac{1}{2} C_{12} \Big\{ \left|\eta_1\right|^2 e^{-\frac{\Gamma_L - \Gamma_S}{2} \cdot (-|\Delta t|)} + \left|\eta_2\right|^2 e^{\frac{\Gamma_L - \Gamma_S}{2} \cdot (-|\Delta t|)} + \\
&\quad - 2 \left|\eta_1\right| \left|\eta_2\right| \cos\left[\Delta m \Delta t + \phi_2 - \phi_1\right] \Big\} \cdot \left[-\frac{2}{\Gamma_L + \Gamma_S} e^{-\frac{\Gamma_L + \Gamma_S}{2} T} \right]_{t=|\Delta t|}^{t=\infty} = \\
&= \frac{C_{12}}{\Gamma_S + \Gamma_L} \Big\{ \left|\eta_1\right|^2 e^{\frac{\Gamma_L - \Gamma_S}{2} |\Delta t|} + \left|\eta_2\right|^2 e^{\frac{\Gamma_S - \Gamma_L}{2} |\Delta t|} + \\
&\quad - 2 \left|\eta_1\right| \left|\eta_2\right| \cos\left[-\Delta m \left|\Delta t\right| + \phi_2 - \phi_1\right] \Big\} e^{-\frac{\Gamma_L + \Gamma_S}{2} |\Delta t|} = \\
&= \frac{C_{12}}{\Gamma_S + \Gamma_L} \Big\{ \left|\eta_1\right|^2 e^{-\Gamma_S |\Delta t|} + \left|\eta_2\right|^2 e^{-\Gamma_L |\Delta t|} + \\
&\quad - 2 \left|\eta_1\right| \left|\eta_2\right| e^{-\frac{\Gamma_L + \Gamma_S}{2} |\Delta t|} \cos\left[\Delta m \left|\Delta t\right| + \phi_1 - \phi_2\right] \Big\}.
\end{aligned}
$$

B Fortran code

B.1 Plotting a normalised function

```
      function wfnorma(dt)
      real gkl,gks,gav,dg,taus,taul,hbar,dm,df
      real alpha,beta,gamma
      real rl,eta,wu,iks,igr,zet,dtm
      real part1,part2,part3,part4,part5
      real np1,np2,np3,np4,np5,norm

      hbar=6.58211915
      taus=0.8958
      taul=511.6
      dm=0.529*hbar
      tcc=taus/hbar
      gks=hbar/taus
      gkl=hbar/taul
      dg=gks-gkl
      gav=(gks+gkl)/2

      alpha=0.0
      beta=0.00
      gamma=0.0000

      pi=4.*atan(1.)
      eta=0.002232
      phi1=43.51*pi/180
      phi2=atan(2*dm/dg)
      df=phi1-phi2
      dvar=sqrt(dm**2+0.25*dg**2)
      rl=eta**2+gamma/dg+4*beta/dg*eta/(dvar**2)
     & *(dm*dg*cos(phi1)+(dm**2)
     & *sin(phi1)-0.25*(dg**2)*sin(phi1))

      igr=gav+alpha-gamma
      iks=igr+gks
      wu=8*beta/(dvar*eta*(iks**2+dm**2))
      zet=rl/(gav*eta**2)

C maximal delta t value:
      dtm=50.

      part1=zet*(exp(-gks*dt*tcc)+exp(-gkl*dt*tcc))

      part2=-2/igr*cos(dm*dt*tcc)*exp(-igr*dt*tcc)

      part3=wu*(iks*sin(dm*tcc*dt+df)
     & +dm*cos(dm*tcc*dt+df))*exp(-igr*tcc*dt)

      part4=wu*(iks*sin(df)+dm*cos(df))*exp(-gks*tcc*dt)
```

```
  part5=-2/gks*(gamma/(dg*eta**2)+2*beta/(dvar*eta)
& *sin(phi1)/cos(phi2))*exp(-gks*tcc*dt)

  np1=zet*(1/(gks*tcc)*(1-exp(-gks*dtm*tcc))
& +1/(gkl*tcc)*(1-exp(-gkl*dtm*tcc)))

  np2=-2/(igr*(igr**2+dm**2)*tcc**2)
& *(igr*tcc+exp(-igr*dtm*tcc)
& *(dm*tcc*sin(dm*dtm*tcc)-igr*tcc*cos(dm*dtm*tcc)))

  np3=wu*iks/((igr*tcc)**2+(dm*tcc)**2)
& *(igr*tcc*sin(df)+dm*tcc*cos(df)-exp(-igr*tcc*dtm)
& *(igr*tcc*sin(dm*tcc*dtm+df)+dm*tcc*cos(dm*tcc*dtm+df)))

  np4=wu*(iks*sin(df)+dm*cos(df))/(gks*tcc)
& *(1-exp(-gks*tcc*dtm))

  np5=-2/(tcc*gks**2)*(gamma/(dg*eta**2)+2*beta/(dvar*eta)
& *sin(phi1)/cos(phi2))*(1-exp(-gks*tcc*dtm))

  norm=np1+np2+np3+np4+np5

  wfnorma=(part1+part2+part3+part4+part5)/norm

  return
  end
```

B.2 Fitting

Fitting was done in PAW (Physics Analysis Workstation). Examples of fortran and kumac files are below.

B.2.1 Fortran file

```
  function fitnorma(dt)
  parameter(nbin=50)
  real teo(nbin),eff(nbin),taul,dtm
  real rl,eta,gks,gkl,dg,dm,gav,pi,dvar
  real help,help1,tcc,hbar,phi1,phi2,df,taus
  real np1,np2,np3,np4,np5,norm

  vector smear
  vector nnbin
  vector effi
  common/pawpar/par(4)

  pi=4.*atan(1.)
  hbar=6.58211915
  taus=0.8958
  taul=511.6
  tcc=taus/hbar
  gks=hbar/taus
```

```
        gkl=hbar/taul
        dg=gks-gkl
        gav=(gks+gkl)/2
        dm=0.529*hbar
        phi1=43.51*pi/180
        phi2=atan(2*dm/dg)
        df=phi1-phi2

        eta=0.002232
        dvar=sqrt(dm**2+0.25*dg**2)
        rl=eta**2+par(4)/dg+4*par(3)/dg
     & *eta/(dvar**2)*(dm*dg*cos(phi1)
     & +(dm**2)*sin(phi1)-0.25*(dg**2)*sin(phi1))

        igr=gav+par(2)-par(4)
        iks=igr+gks
        wu=8*par(3)/(dvar*eta*(iks**2+dm**2))
        zet=rl/(gav*eta**2)

C maximal delta t value:
        dtm=12.

        np1=zet*(1/(gks*tcc)*(1-exp(-gks*dtm*tcc))
     & +1/(gkl*tcc)*(1-exp(-gkl*dtm*tcc)))

        np2=-2/(igr*(igr**2+dm**2)*tcc**2)
     & *(igr*tcc+exp(-igr*dtm*tcc)
     & *(dm*tcc*sin(dm*dtm*tcc)-igr*tcc*cos(dm*dtm*tcc)))

        np3=wu*iks/((igr*tcc)**2+(dm*tcc)**2)
     & *(igr*tcc*sin(df)+dm*tcc*cos(df)-exp(-igr*tcc*dtm)
     & *(igr*tcc*sin(dm*tcc*dtm+df)+dm*tcc*cos(dm*tcc*dtm+df)))

        np4=wu*(iks*sin(df)+dm*cos(df))/(gks*tcc)
     & *(1-exp(-gks*tcc*dtm))

        np5=-2/(tcc*gks**2)*(gamma/(dg*eta**2)+2*beta/(dvar*eta)
     & *sin(phi1)/cos(phi2))*(1-exp(-gks*tcc*dtm))

        norm=np1+np2+np3+np4+np5

        binw=50./nbin
        nnbb=nnbin(1)
        write(6,*)(par(i),i=1,4)
        nowa=0.
        aidt=0.
        i=int(dt/binw)+1
        do j=1,nbin
          if(smear(j,i).gt.0) then
          dt1=binw*(j-0.5)
          teo(j)=
     & par(1)/norm
```

```
     & *(rl/(gav*eta**2)*(1/(gks*tcc)*(exp(-gks*tcc*(j-1))
     & -exp(-gks*tcc*j))+1/(gkl*tcc)*(exp(-gkl*tcc*(j-1))
     & -exp(-gkl*tcc*j)))
     & -2/(igr*(igr**2+dm**2)*tcc**2)
     & *(exp(-igr*tcc*j)*(dm*tcc*sin(dm*tcc*j)-igr*tcc
     & *cos(dm*tcc*j))-exp(-igr*tcc*(j-1))*(dm*tcc
     & *sin(dm*tcc*(j-1))-igr*tcc*cos(dm*tcc*(j-1))))
     & +wu/((igr**2+dm**2)*tcc**2)
     & *(iks*(exp(-igr*tcc*(j-1))*(igr*tcc
     & *sin(dm*tcc*(j-1)+df)+dm*tcc*cos(dm*tcc*(j-1)+df))
     & -exp(-igr*tcc*j)*(igr*tcc*sin(dm*tcc*j+df)
     & +dm*tcc*cos(dm*tcc*j+df)))
     & +dm*(exp(-igr*tcc*(j-1))*(igr*tcc
     & *cos(dm*tcc*(j-1)+df)-dm*tcc*sin(dm*tcc*(j-1)+df))
     & +exp(-igr*tcc*j)*(-igr*tcc*cos(dm*tcc*j+df)
     & +dm*tcc*sin(dm*tcc*j+df))))
     & +wu/(gks*tcc)*(iks*sin(df)+dm*cos(df))
     & *(exp(-gks*tcc*(j-1))-exp(-gks*tcc*j))
     & -2/(tcc*gks**2)*(par(4)/(dg*eta**2)
     & +2*par(3)/(dvar*eta)*sin(phi1)/cos(phi2))
     & *(exp(-gks*tcc*(j-1))-exp(-gks*tcc*j)))

         aidt=aidt+effi(j)*smear(j,i)*teo(j)
         endif
       end do

       fitnorma=aidt
       return
       end
```

B.2.2 Kumac file

```
for/fil 67 fitnorma.ps
opt nsta
opt fit
set fit 1111111111
h/fil 1 tt.hbook
set hcol 1
set mtyp 20
k=50
ve/cre nnbin(1) r 4
|ve/cre tmax(1) r 30
ve/cre tmax(1) r 12
ve/cre smear([k],[k]) r
ve/rea smear newsmear_chi15_1ts_full.dat
ve/cre effi([k]) r
|ve/rea effi ./neweff/eff_chi15_0.25ts.txt
ve/rea effi eff_corr_chi15_1ts_full.txt
ve/cre par(4) r 120000. 0. 0. 0.
ve/cre step(4) r 300 0.0000001 0.0000001 0.0000001
ve/cre pmin(4) r 5000. -9.4 -0.4 -0.4
ve/cre pmax(4) r 200000. 10.0 0.4 0.4
```

```
ve/cre errpar(4) r
h/fit 118(0.:12.) fitnorma.f SBLE 4 par step pmin pmax errpar
h/plo 118(0.:12.) e
graphics/hplot/atitle '[D]t, [t]?S!' 'number of events'
meta 0
close 67
```

References

[1] T. D. Lee and C.-N. Yang. *Question of Parity Conservation in Weak Interactions.* Phys. Rev., **104**: 254–258, 1956.

[2] J. H. Christenson, J. W. Cronin, V. L. Fitch, and R. Turlay. *Evidence for the 2π Decay of the K_2^0 Meson.* Phys. Rev. Lett., **13**: 138–140, 1964.

[3] A. Angelopoulos et al. *First direct observation of time-reversal non-invariance in the neutral kaon system.* Phys. Lett. B, **444**: 43–51, 1998.

[4] W. Pauli. *Exclusion principle, Lorentz group and reflexion of space-time and charge* in *Niels Bohr and the development of physics,* edited by W. Pauli. Pergamon, London, 1955, p. 30.

[5] G. Lüders. *Proof of the TCP theorem.* Ann. of Phys., **2**: 1–15, 1957. Reprinted in Ann. of Phys. **281**: 1004-1018, 2000.

[6] T. D. Lee. *Particle Physics and Introduction to Field Theory.* Newark: Harwood Academic Publishers, 1981.

[7] A. Di Domenico. *Neutral kaon interferometry at a ϕ-factory* in *Handbook on neutral kaon interferometry at a Φ-factory,* edited by A. Di Domenico, Frascati Physics Series Vol. **XLIII**: 1-38, 2007.

[8] V. Weisskopf and E. P. Wigner. *Calculation of the natural brightness of spectral lines on the basis of Dirac's theory.* Z. Phys., **63**: 54–73, 1930.

[9] G. V. Dass and W. Grimus. *Testing the Weisskopf-Wigner approximation by using neutral meson antimeson correlated states* and references therein. Phys. Lett. B, **521**: 267–272, 2001.

[10] M. Fidecaro and H.-J. Gerber. *The fundamental symmetries in the neutral kaon system: A pedagogical choice.* Rept. Prog. Phys., **69**: 1713–1770, 2006.

[11] L. Maiani. *CP and CPT Violation in Neutral Kaon Decays,* in *The 2nd DAΦNE Physics Handbook,* edited by L. Maiani, G. Pancheri and N. Paver, Vol. I, INFN-LNF, Frascati, 1995.

[12] C. Amsler *et al.* (Particle Data Group). *Review of Particle Physics.* Phys. Lett. B, **667**: 1, 2008, and partial update for 2010 edition (URL: http://pdg.lbl.gov).

[13] C. Buchanan, R. Cousins, C. Dib, R. D. Peccei, and J. Quackenbush. *Testing CP and CPT violation in the neutral kaon system at a ϕ factory.* Phys. Rev. D, **45**: 4088–4107, 1992.

[14] A. Einstein, B. Podolsky, and N. Rosen. *Can quantum mechanical description of physical reality be considered complete?* Phys. Rev., **47**: 777–780, 1935.

[15] E. Schrödinger. *Discussion of probability relations between separated systems.* Proc. Cambr. Phil. Soc., **31**: 555–563, 1935.

[16] J. Bub. *Quantum Entanglement and Information,* in *The Stanford Encyclopedia of Philosophy,* edited by E. N. Zalta, edition Fall 2010. url: http://plato.stanford.edu/archives/fall2010/entries/qt-entangle/ and links therein.

[17] R. A. Bertlmann, W. Grimus, and B. C. Hiesmayr. *Quantum mechanics, Furry's hypothesis and a measure of decoherence in the K^0 $\bar{K}^0$ system.* Phys. Rev. D, **60**: 114032, 1999.

[18] A. Di Domenico and KLOE collaboration. *CPT Symmetry and Quantum Mechanics Tests in the Neutral Kaon System at KLOE.* Found. Phys., **40**: 852–866, 2010.

[19] S. W. Hawking. *Particle Creation by Black Holes.* Commun. Math. Phys., **43**: 199–220, 1975.

[20] For example: S. W. Hawking. *The Unpredictability of Quantum Gravity.* Commun. Math. Phys., **87**: 395–415, 1982.

[21] R. M. Wald. *Quantum gravity and time reversibility.* Phys. Rev. D, **21**: 2742–2755, 1980.

[22] J. R. Ellis, J. S. Hagelin, D. V. Nanopoulos, and M. Srednicki. *Search for Violations of Quantum Mechanics.* Nucl. Phys. B, **241**: 381, 1984.

[23] P. Huet and M.E. Peskin. *Violation of CPT and quantum mechanics in the K^0 - $\bar{K}^0$ system.* Nucl. Phys. B, **434**: 3–38, 1995.

[24] A. Aloisio *et al.* (KLOE collaboration). *The KLOE detector: technical proposal.* LNF-93-002-IR.

[25] F. Bossi, E. De Lucia, J. Lee-Franzini, S. Miscetti, M. Palutan and KLOE collaboration. *Precision Kaon and Hadron Physics with KLOE.* Riv. Nuovo Cim., **31**: 531–623, 2008.

[26] KLOE experiment webpages, http://www.lnf.infn.it/kloe/ and links therein.

[27] DAΦNE webpages, http://www.lnf.infn.it/acceleratori/ and links therein.

[28] G. Amelino-Camelia et al. Physics with the KLOE-2 experiment at the upgraded DAϕNE. *Eur. Phys. J. C*, **68**: 619–681, 2010.

[29] J. Lee-Franzini and P. Franzini. *A flavor of KLOE.* Acta Phys. Polon. B, **38**: 2703–2730, 2007.

[30] KLOE Collaboration. Draft version of *Expression of Interest for the continuation of the KLOE physics program at DAΦNE upgraded in luminosity and in energy,* 2006. Available at http://www.lnf.infn.it/lnfadmin/direzione/roadmap/LoIKLOE.pdf.

[31] D. Leone. *Measurement of the hadronic cross-section $\sigma\left(e^+e^- \to \pi^+\pi^-\right)$ with the KLOE detector using radiative return with tagged photons.* PhD thesis, Karlsruhe University, Germany, 2007.

[32] J. Zdebik. *Merging and splitting of clusters in the electromagnetic calorimeter of the KLOE detector.* Master thesis, Jagiellonian University, Cracow, Poland, 2008.

[33] A. De Santis. *Study of the $e^+e^- \to \omega\pi^0$ process in the ϕ mass region with the KLOE experiment.* PhD thesis, Sapienza University of Rome, Italy, 2008.

[34] M. Adinolfi et al. *The KLOE electromagnetic calorimeter.* Nucl. Instr. and Meth. A, **494**: 326–331, 2002.

[35] KLOE-2 collaboration. *Technical Design Report of the Inner Tracker for the KLOE-2 experiment.* 2010.

[36] S. Cerioni. *Inner Tracker, Layout–Integration–Installation study.* Presented at General Meeting INFN-Bari, 2009.

[37] F. Sauli. *GEM: A new concept for electron amplification in gas detectors.* Nucl. Instrum. Meth. A, **386**: 531–534, 1997.

[38] E. De Lucia. *Physics simulation studies.* Presented at General Meeting INFN-Bari, 2009.

[39] KLOE-2 collaboration. *A proposal for the roll-in of the KLOE-2 detector.* LNF-07/19 (IR), 2007.

[40] The KLOE-LNF Collaboration and the KLOE-LNF Technical Staff. *KLOE / KLOE-2.* Unpublished, available at http://www.lnf.infn.it/rapatt/2009/1/KLOE:KLOE2.pdf.

[41] F. Happacher, M. Martini, S. Miscetti, and I. Sarra. *Tile and crystal calorimeter for KLOE-2 experiment.* Nucl. Phys. Proc. Suppl., **197**: 215–218, 2009.

[42] M. Cordelli et al. *Test of a LYSO matrix with an electron beam.* Nucl. Instr. and Meth. A, **617**: 109–112, 2010.

[43] M. Cordelli et al. *QCALT: a tile calorimeter for KLOE-2 upgrade.* Nucl. Instr. Meth. A, **617**: 105–106, 2010.

[44] F. Gonella. *The High Energy Tagger for $\gamma\gamma$ physics at KLOE-2.* Presented at 11^{th} ICATPP, 2009.

[45] D. Babusci *et al. The low energy tagger for the KLOE-2 experiment.* Nucl. Instr. and Meth. A, **617**: 81–84, 2010.

[46] F. Archilli *et al. Gamma-gamma tagging system for KLOE2 experiment.* Nucl. Instr. and Meth. A, **617**: 266–268, 2010.

[47] A. De Santis, private communication 2010.

[48] A. De Santis. *Lorentz invariance violation: vertex resolution study.* KLOE-2 private document, 2010.

[49] R. Adler *et al. Test of CPT Symmetry and Quantum Mechanics with Experimental data from CPLEAR.* Phys. Lett. B, **364**: 239–245, 1995.

[50] Y. Liu, J.-L. Chen, and M.-L. Ge. *A constraint on EHNS parameters from solar neutrino problem.* J. Phys. G, **24**: 2289–2296, 1998.